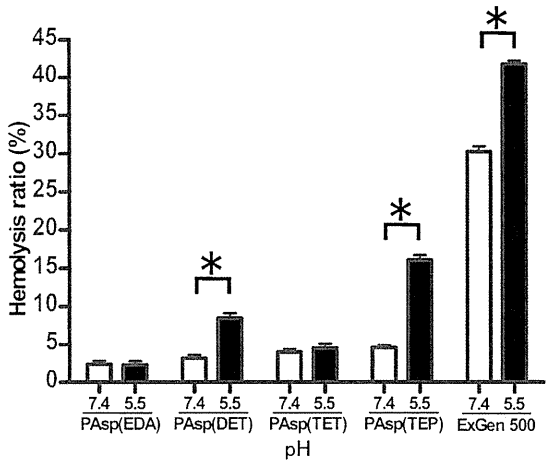

Figure 4. Hemolytic activity of PAsp(EDA), PAsp(DET), PAsp(TET), PAsp(TEP), and ExGen 500 ([amine] = 5 mM) against murine erythrocytes at pH 7.4 and 5.5. Results are expressed as mean ± SEM ($N = 4$). *$P < 0.05$.

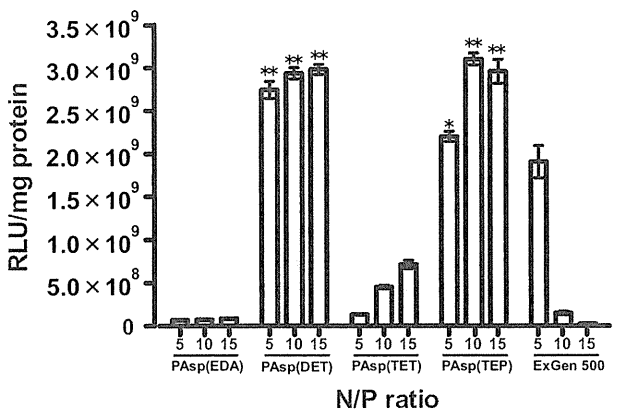

Figure 5. In vitro transfection efficiency of PAsp(EDA), PAsp(DET), PAsp(TET), PAsp(TEP), and ExGen 500 polyplexes at varying N/P ratios with Huh-7 cells determined by luciferase assay. Results are expressed as mean ± SEM ($N = 4$). * indicates that polyplexes show a significantly higher transfection efficiency than the PA-Os polyplexes at the same N/P ratio ($P < 0.01$), ** indicates that polyplexes show a significantly higher transfection efficiency than the PA-Os polyplexes at the same N/P ratio ($P < 0.01$) and the ExGen 500 polyplexes at N/P = 5 ($P < 0.05$).

activities of the polyplexes from the N-substituted polyaspartamides and ExGen 500 were determined at N/P = 10, which corresponds to the residual molar ratio of the amino groups in polycations to the phosphate groups in pDNA (Figure 1, Supporting Information). The hemolytic activity of polyplexes showed a similar odd−even effect, indicating that the membrane-destabilizing activity of the polycations was maintained even after the formation of polyplexes.

Size and ζ-Potential of Polyplexes Prepared from pDNA and N-Substituted Polyaspartamides. The polyplexes from the N-substituted polyaspartamides were characterized by measuring the ζ-potential and hydrodynamic diameter at pH 7.4 and 37 °C (Figure 2, Supporting Information). At N/P ratios above 4, all polyplexes had a similar size of approximately 100 nm with a

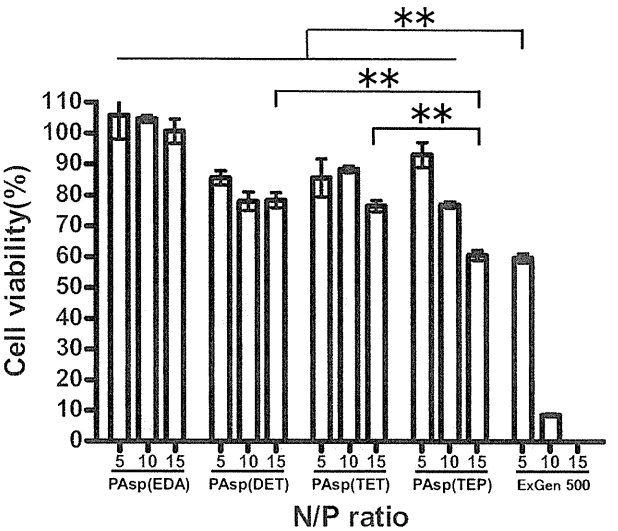

Figure 6. Cell viability assay of Huh-7 cells incubated with PAsp(EDA), PAsp(DET), PAsp(TET), PAsp(TEP), and ExGen 500 polyplexes under the same experimental conditions as in Figure 5. Results are expressed as mean ± SEM ($N = 4$). **$P < 0.01$.

constant ζ-potential of approximately 30 mV. Note that the formation of large aggregates around 1 μm was observed in each polyplex at a specific N/P ratio. Because each polyplex exhibited a ζ-potential close to neutral at this N/P ratio, large aggregate formation is expected to be due to decreased colloidal stability induced by charge neutralization. In the following experiments, the polyplexes prepared at N/P ratios above 4 were used because they apparently have similar physicochemical characteristics.

In Vitro Transfection and Cytotoxicity. The transfection efficiency of the luciferase gene in human hepatoma cells (Huh-7) was compared among the polyplexes prepared from PAsp(EDA), PAsp(DET), PAsp(TET), and PAsp(TEP) at N/P = 5, 10, and 15 (Figure 5). The polyplex from a linear PEI-based commercial transfection reagent (ExGen 500) was used as a control. Remarkable transfection efficiencies, which were higher than the maximum value obtained by ExGen 500 at N/P = 5, were achieved by polyplexes from PAsp(DET) (over N/P = 5) and PAsp(TEP) (over N/P = 10) possessing the even-numbered repeating aminoethylene units (PA-Es) ($P < 0.05$). Furthermore, polyplexes from PA-Es [PAsp(DET) and PAsp(TEP)] revealed significantly higher transfection efficiencies than those from PA-Os [PAsp(EDA) and PAsp(TET)] at all of the examined N/P ratios ($P < 0.01$). This remarkable odd−even effect on transfection efficiencies was not only limited to Huh-7 cells but was also observed for a human lung adenocarcinoma epithelial cells (A549) and a human umbilical vein endothelial cells (HUVEC) (Figure 3, Supporting Information). Note that a drastic reduction in the transfection efficiency was observed for the ExGen 500 polyplexes at higher N/P ratios, whereas it was not observed for any polyplexes from the N-substituted polyaspartamides. The substantially decreased transfection efficiency in the ExGen 500 polyplexes at higher N/P ratios is believed to be a direct result of severe cytotoxicity, as shown in Figure 6. In contrast, all polyplexes from the N-substituted polyaspartamides maintained a cell viability over 85% at N/P = 5 and over 75% even at N/P = 15, except for the polyplex from PAsp(TEP) at N/P = 15 (60%). Indeed, significant differences between the polyplexes from ExGen 500 at

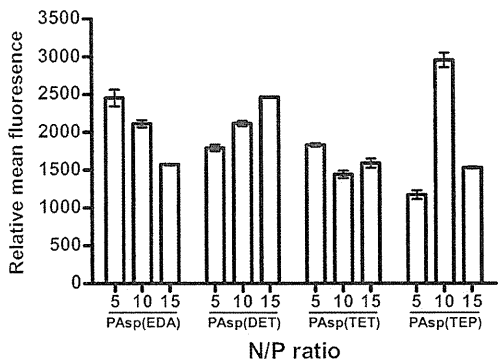

Figure 7. Cellular uptake of Cy5-labeled pDNA complexed with N-substituted polyaspartamides at various N/P ratios after 24 h incubation with Huh-7 cells (10 000 cells). Results are expressed as mean ± SEM ($N = 4$).

N/P = 5 and other N-substituted polyaspartamides except PAsp(TEP) at N/P = 15 were observed ($P < 0.01$). Polyplexes from PAsp(TEP) showed significantly lower cell viability than those from PAsp(DET) and PAsp(TET) at N/P = 15 ($P < 0.01$), indicating higher cytotoxicity with an increase in the N/P ratio.

Cellular Uptake of Polyplexes Determined by Flow Cytometry. The transfection efficiency of the polyplexes is often correlated with their cellular uptake. Thus, we compared the cellular uptake of each polyplex containing Cy5-labeled pDNA using flow cytometry. The histogram of flow cytometry revealed that almost 100% of the cells underwent polyplex uptake (data not shown). Figure 7 shows the relative mean fluorescence for the cellular uptake of Cy5-labeled pDNA, which apparently does not correlate with the transfection efficiency (Figure 5). Indeed, despite the significantly lower transfection efficiency, the polyplexes from PAsp(EDA) and PAsp(TET) showed levels of cellular uptake similar to those from PAsp(DET) and PAsp(TEP).

Intracellular Trafficking of Polyplexes Observed by Confocal Laser Scanning Microscopy (CLSM). Intracellular trafficking of each polyplex (N/P = 10) containing Cy5-labeled pDNA (red) was monitored particularly for endosomal localization by CLSM after staining the late endosome and lysosome with LysoTracker Green (green) and the nucleus with Hoechst 33342 (blue) (Figure 8a,b). In the overlay images, the yellow pixels represent the colocalization of Cy5-labeled pDNA with the late endosome/lysosome. Note that in our previous CLSM study Cy5-labeled pDNA in the poly(L-lysine) polyplex, which was used as the negative control and lacks endosomal escape ability, was found to maintain colocalization with the late endosome/lysosome throughout the observation period. This result provided the basis for estimating the endosomal escape ability of examined polyplexes from the decrease in the colocalization ratio estimated from the CLSM data.[26] Eventually, PAsp(DET) and PAsp(TEP) polyplexes appeared to disperse more efficiently in the entire cytoplasmic region than other polyplexes from the polymers with the odd-numbered repeating aminoethylene units in the side chains. As shown in Figure 8c, PAsp(EDA) and PAsp(TET) polyplexes showed an increase in the colocalization ratio until 12 and 24 h, respectively, indicating that the major fraction of PA-O polyplexes might be trapped in the lysosome. In contrast, PAsp(DET) and PAsp(TEP) polyplexes showed colocalization ratios lower than those of PAsp(EDA) and PAsp(TET) polyplexes at all time points. Also, PAsp(DET) and PAsp(TEP) polyplexes showed a decrease in the colocalization ratio after 12 and 6 h incubation, respectively, suggesting that the major fraction of PA-E polyplexes might escape from the endosome. At 12 h, the colocalization ratio of PAsp(DET) polyplexes was significantly lower than those of PAsp(EDA) and PAsp(TET) polyplexes ($P < 0.05$). At 24 and 48 h, the colocalization ratio of PAsp(TEP) polyplexes was significantly lower than that of PAsp(DET) polyplexes ($P < 0.05$ at 24 h, $P < 0.01$ at 48 h), indicating that the most efficient endosomal escape was for PAsp(TEP) polyplexes. Furthermore, the Manders coefficients were calculated using Image J software (http://rsbweb.nih.gov/ij/) to evaluate the colocalization of Cy5-labeled pDNA and LysoTracker after 48 h incubation. Note that the coefficients range between 0 and 1, which indicates no overlap and full overlap, respectively, and a higher value indicates that a larger fraction of polyplexes is trapped in the endosome/lysosome. The coefficients were calculated to be 0.549 for PAsp(EDA), 0.381 for PAsp(DET), 0.498 for PAsp(TET), and 0.345 for PAsp(TEP), consistent with the endosome colocalization ratios in Figure 8c. From these results, we conclude that the polyplexes from the polymer possessing the even-numbered repeating aminoethylene units enable the efficient endosomal escape of complexed pDNA into the cytoplasm, which agrees well with the transfection results shown in Figure 5.

DISCUSSION

In this study, to elucidate the precise structure–function relationship of the polyplexes, we synthesized a series of N-substituted polyaspartamides with increasing numbers of repeating aminoethylene units in the side chain: PAsp(EDA), PAsp(DET), PAsp(TET), and PAsp(TEP) (one to four repeating aminoethylene unit(s), respectively). The polyplexes from these N-substituted polyaspartamides were confirmed to have a similar size (~100 nm) and ζ-potential (~30 mV) at N/P ratios >4 (Figure 2, Supporting Information), suggesting similar fundamental physicochemical properties. The in vitro transfection experiment with Huh-7 cells exhibited a distinctive odd–even effect with respect to the number of repeating aminoethylene units: the polyplexes from the polymer with the even-numbered repeating aminoethylene units (PA-E) showed appreciably higher transfection efficiencies without marked cytotoxicity compared to polymers with odd-numbered repeating aminoethylene units (PA-O) (Figures 5 and 6).

To elucidate the reasons for this unique odd–even effect, we examined the cytotoxicity, cellular uptake, and endosomal escape behaviors of each polyplex. While the cell viability (Figure 6) and cellular uptake (Figure 7) profiles were similar between the polyplexes from both PA-E and PA-O, a significant difference in the endosomal escape behavior as determined from CLSM imagery was observed between the two variants. PA-E [PAsp(DET) and PAsp(TEP)] polyplexes revealed lower endosomal colocalization and higher dispersion into the cytoplasm than PA-O [PAsp(EDA) and PAsp(TET)] polyplexes (Figure 8), indicating that the higher transfection efficiency of the PA-E polyplexes is strongly correlated with their capability of endosomal escape.

Several previous studies revealed that the endosomal escape of the polyplexes may be facilitated by an increased osmotic pressure in the endosome because of a buffering effect associated with the amino groups in the constituent polycations (proton sponge hypothesis).[12,17] Accordingly, we examined the relationship between the buffering capacity of amino groups in the

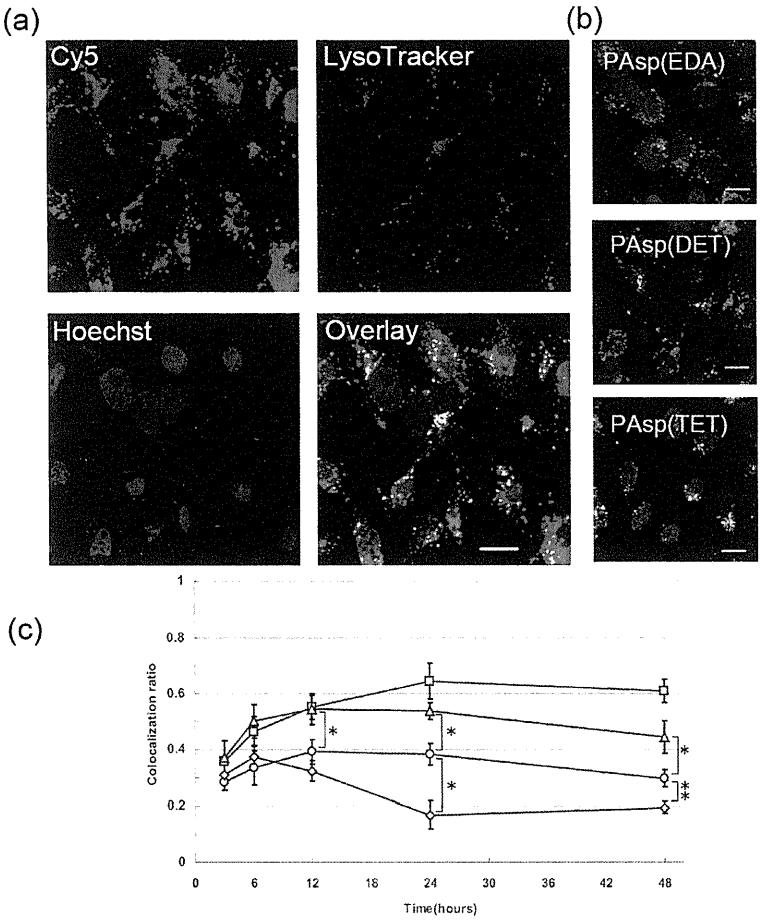

Figure 8. (a) Intracellular distribution of Cy5-labeled pDNA (red) complexed with PAsp(TEP) at N/P = 10 for Huh-7 cells after 48 h incubation. Acidic late endosomes and lysosomes were stained with LysoTracker Green (green). The nuclei were stained with Hoechst 33342 (blue). The scale bar represents 20 μm. (b) Overlay images of Cy5-labeled pDNA, LysoTracker Green, and Hoechst 33342 in Huh-7 transfected with the polyplexes from PAsp(EDA), PAsp(DET), and PAsp(TET) observed under the same conditions as those of part a. (c) Time-dependent changes in colocalization ratios of the PAsp(EDA) (square), PAsp(DET) (circle), PAsp(TET) (triangle), and PAsp(TEP) (diamond) polyplexes containing Cy5-labeled pDNA with late endosomes and lysosomes. Results are expressed as mean ± SEM (N = 10). $^{*}P < 0.05$, $^{**}P < 0.01$.

N-substituted polyaspartamides and the endosomal escape efficiency of their polyplexes. The buffering capacity was estimated from the change in the degree of protonation between pH 7.4 and 5.5 ($\Delta\alpha$) (Table 1) and was consistent with the observed odd−even effect. PA-Es [$\Delta\alpha$ = 0.31 and 0.19 for PAsp(DET) and PAsp(TEP), respectively] possess higher buffering capacities than PA-Os [$\Delta\alpha$ = 0.06 and 0.11 for PAsp(EDA) and PAsp(TET), respectively]. The assumed protonated structures of the side chains for each polymer (Figure 3) are rather interesting. Almost all the amino groups in the PAsp(EDA) side chains are protonated, regardless of pH (7.4 or 5.5). On the other hand, most of the PAsp(DET) side chains are in the monoprotonated state at pH 7.4 (α = 0.51) and diprotonated state at pH 5.5 (α = 0.82) owing to the appreciable difference in pK_{a_1} (8.9) and pK_{a_2} (6.2), as reported in our previous paper.[26] Low pK_{a_2} values in PAsp(DET) are due to the thermodynamic disadvantages of the diprotonated structure in 1,2-diaminoethane caused by electrostatic repulsion between the two protonated amines, locking the conformation in the *anti* form with less rotational freedom (butane effect). The absence of a significant change in α for PAsp(TET) with pH ($\Delta\alpha$ = 0.11) may be explained in a similar way: the fully protonated (triprotonated) structure of an *N*-(2-aminoethyl)-1,2-diaminoethane unit has a substantial thermodynamic penalty because of the strong repulsive force from the two neighboring protonated amines. Consequently, the side chain prefers to exist as a diprotonated structure with diethyleneamine spacing ($-NH_2^+-CH_2-CH_2-NH-CH_2-CH_2-NH_3^+$) containing a nonprotonated amino group in the center even at lower pH. Alternatively, for PAsp(TEP), α increases from 0.49 to 0.68 with a decrease in pH from 7.4 to 5.5 because the pK_{a_3} value (6.3) exists between these two pH values. As shown in Figure 3, the dominant structure changes from a diprotonated state at pH 7.4 to a triprotonated state at pH 5.5. The latter form, with its integrated positive charge, is still allowed under acidic conditions possibly because the increase in electrostatic repulsion accompanying the third protonation may be alleviated by sufficient length and rotational flexibility of the diethyeleneamine spacing ($-CH_2CH_2NHCH_2CH_2-$). Note that pK_{a_4} of PAsp(TEP) is much lower than the titration range (pH < 1.2) because of the highly repulsive nature of the fully protonated structure.

Although the buffering capacity may explain the odd−even effect observed in the transfection efficiency of the examined

polyplexes, it does not completely agree with the order of their endosomal escape efficiency. PAsp(DET) possessed relatively larger $\Delta\alpha$ than PAsp(TEP); however, the polyplex from the latter achieved significantly higher endosomal escape efficiency (lower endosomal colocalization ratio) than that from the former (Figure 8), suggesting the presence of an additional factor affecting the endosomal escape behavior of the polyplexes. In this regard, membrane destabilization directly by polycation interaction should be emphasized, as indicated from the result of the hemolysis assay shown in Figure 4. The odd−even effect was clearly observed in this assay and only the PA-E series induced a substantial increase in hemolysis at acidic pH. PAsp(TEP) demonstrated the highest hemolysis (14.4%), followed by PAsp(DET) (8.0%), PAsp(TET) (4.9%), and PAsp(EDA) (1.8%). The order of hemolytic activity at pH 5.5 agrees well with the endosomal escape efficiency of the polyplexes (Figure 8), suggesting that disturbing the membrane integrity may be important for the endosomal escape of these polyplexes. Furthermore, the weak hemolytic activity for each polymer at pH 7.4 agrees with their low cytotoxicity (Figure 6), suggesting their limited interaction with plasma membranes of mammalian cells under physiological conditions. Note that ExGen 500 also showed the membrane destabilizing activity in response to the acidic pH in the endosome (Figure 4). Nevertheless, it is assumed that the considerably high hemolytic activity (approximately 30%) of ExGen 500 at pH 7.4 may be correlated with its high cytotoxicity (Figure 6), suggesting that the augmentation of repeating aminoethylene units might increase cytotoxicity regardless of pH.

To further discuss the mechanism for cellular membrane destabilization induced by the N-substituted polyaspartamides, we focus here on the number of protonated amines (NA) and the overall cationic charge density (CD) in each polymer strand (Table 1). A previous study revealed that polycations with larger NA and higher CD tend to induce stronger disturbances in the membrane integrity, presumably resulting from a higher affinity of the plasma membrane for positively charged components.[33] Yet the calculated NA and CD were apparently not correlated with the hemolytic activity and simply increased with the number of aminoethylene units without any odd−even effects.

Next, we investigated whether the protonation state of the N-substituted polyaspartamides (Figure 3) would contribute to the odd−even effect from the viewpoint of specific interactions that may lead to a disturbance in the membrane integrity. It is interesting to consider that PA-Es [PAsp(DET) and PAsp(TEP), Figure 3] at pH 5.5 contain a diprotonated state of the diaminoethane unit ($-NH_2^+-CH_2-CH_2-NH_2^+-$), corresponding to their strong hemolytic activity in acidic conditions. In contrast, no such structure is determined for PA-Os [PAsp(EDA) and PAsp(TET)] at either pH 7.4 nor 5.5 nor for PA-Es at pH 7.4, and eventually they have very limited hemolytic activity. In particular, for PAsp(TET) at pH 7.4/5.5 and PAsp(TEP) at pH 7.4, two protonated amines are spatially separated by diethyleneamine ($-CH_2-CH_2-NH-CH_2-CH_2-$) or *N,N′*-ethylene-1,2-diaminoethane ($-CH_2-CH_2-NH-CH_2-CH_2-NH-CH_2-CH_2-$) spacers. It is likely that a critical spacing length between the two protonated amino groups may exist in order to induce an effective membrane interaction. Note that an N-substituted polyaspartamide possessing a 1,3-diaminopropane unit ($-NHCH_2CH_2CH_2NH-$) in the side chain [PAsp(DPT)] assumed a fully protonated structure at pH 7.4/5.5 and induced substantial membrane destabilization of mammalian cells, as previously reported.[26] It can be assumed that two positively charged units may need to be close to each other via a spacing equivalent of approximately two or three methylene units to exert a strong interaction with cellular membranes. The additional positively charged unit in the side chain of PAsp(TEP), separated from the diprotonated diamine unit ($-NH_2^+-CH_2-CH_2-NH_2^+-$) by a flexible $-CH_2-CH_2-NH-CH_2-CH_2-$ spacer, may contribute further to enhance the binding affinity through the formation of a polyvalent charged array as multiple binding sites. This multiple binding scheme reasonably explains PAsp(TEP) polyplex's higher hemolysis efficiency as well as its enhanced endosomal escape capability compared to that of PAsp(DET) polyplex, even though the former has a lower buffering capacity than the latter.

CONCLUSION

Efficient transfection without severe cytotoxicity was achieved by the polyplexes from the N-substituted polyaspartamides possessing the even-numbered repeating aminoethylene units in their side chains [PAsp(DET) and PAsp(TEP)]. This agrees with their appreciably high buffering capacity as well as their capability to disturb the membrane integrity selectively at endosomal pH, thereby facilitating the endosomal escape of the polyplexes. Results of the hemolysis assay and the CLSM observations tracking subcellular distribution of the polyplexes suggest that two protonated amino groups may need to be tethered with critical spacing equivalent to approximately two or three methylene units to induce the strong interaction of polycations in the polyplexes with the endosomal membrane, leading to their effective transport into the cytoplasm. Importantly, fine-tuning of the number, spacing, and protonation status of repetitive amine units in the polycation side chain, as reported in this study, resolves the conflict between endosomal escape and cytotoxicity of the polyplexes, thus providing a new design concept for nonviral gene delivery systems directed toward clinical applications.

ASSOCIATED CONTENT

Supporting Information. Experimental Section and supplemental Figures 1−3. This material is available free of charge via the Internet at: http://pubs.acs.org

AUTHOR INFORMATION

Corresponding Author
kataoka@bmw.t.u-tokyo.ac.jp

ACKNOWLEDGMENT

This work was financially supported in part by the Center for Medical System Innovation (CMSI) and the Funding Program for World-Leading Innovative R&D on Science and Technology (FIRST) from Japan Society for the Promotion of Science (JSPS) and the Core Research Program for Evolutional Science and Technology (CREST) from Japan Science and Technology Agency (JST). The authors thank Kotoe Date (The University of Tokyo) for her technical assistance.

REFERENCES

(1) Mastrobattista, E.; van der Aa, M. A.; Hennink, W. E.; Crommelin, D. J. A. *Nat. Rev. Drug Discovery* **2006**, *5*, 115–121.
(2) Mintzer, M. A.; Simanek, E. E. *Chem. Rev.* **2009**, *109*, 259–302.

(3) Pack, D. W.; Hoffman, A. S.; Pun, S. *Nat. Rev. Drug Discovery* **2005**, *4*, 581–593.
(4) Wood, K. C.; Little, S. R.; Langer, R.; Hammond, P. T. *Angew. Chem., Int. Ed.* **2005**, *44*, 6704–6708.
(5) Zugates, G. T.; Anderson, D. G.; Little, S. R.; Lawhorn, I. E. B.; Langer, R. *J. Am. Chem. Soc.* **2006**, *128*, 12726–12734.
(6) Srinivasachari, S.; Fichter, K. M.; Reineke, T. M. *J. Am. Chem. Soc.* **2008**, *130*, 4618–4627.
(7) Green, J. J.; Langer, R.; Anderson, D. G. *Acc. Chem. Res.* **2008**, *41*, 749–759.
(8) Schaffert, D.; Troiber, C.; Salcher, E. E.; Frohlich, T.; Martin, I.; Badgujar, N.; Dohmen, C.; Edinger, D.; Klager, R.; Maiwald, G.; Farkasova, K.; Seeber, S.; Jahn-Hofmann, K.; Hadwiger, P.; Wagner, E. *Angew. Chem., Int. Ed.* **2011**, *50*, 1–4.
(9) Wattiaux, R.; Laurent, N.; Coninck, W. N.; Jadot, M. *Adv. Drug Delivery Rev.* **2000**, *41*, 201–208.
(10) Wagner, E.; Plank, C.; Zatloukal, K.; Cotton, M.; Birnstiel, M. L. *Proc. Natl. Acad. Sci. U. S. A.* **1992**, *89*, 7934–7938.
(11) Haensler, J.; Szoka, F. C. *Bioconjugate Chem.* **1993**, *4*, 372–379.
(12) Boussif, O.; Lezoualc'h, F.; Zanta, M. A.; Mergny, M. D.; Scherman, D.; Demeneix, B.; Behr, J. P. *Proc. Natl. Acad. Sci. U. S. A.* **1995**, *92*, 7297–7301.
(13) Midoux, P.; Monsigny, M. *Bioconjugate Chem.* **1999**, *10*, 406–411.
(14) Thomas, M.; Kilbanov, A. M. *Proc. Natl. Acad. Sci. U. S. A.* **2002**, *99*, 14640–14645.
(15) Kwon, E. J.; Bergen, J. M.; Pun, S. H. *Bioconjugate Chem.* **2008**, *19*, 920–927.
(16) Hunter, A. C. *Adv. Drug Delivery Rev.* **2006**, *58*, 1523–1531.
(17) Neu, M.; Fischer, D.; Kissel, T. *J. Gene Med.* **2005**, *7*, 992–1009.
(18) Ferrari, S.; Moro, E.; Pettenazzo, A.; Behr, J. P.; Zacchello, F.; Scarpa, M. *Gene Ther.* **1997**, *4*, 1100–1106.
(19) Wightman, L.; Kircheis, R.; Rossler, V.; Carotta, S.; Ruzicka, R.; Kursa, M.; Wagner, E. *J. Gene Med.* **2001**, *3*, 362–372.
(20) Itaka, K.; Harada, A.; Yamasaki, Y.; Nakamura, K.; Kawaguchi, H.; Kataoka, K. *J. Gene Med.* **2004**, *6*, 76–84.
(21) Densmore, C. L.; Kleinerman, E. S.; Gautam, S.; Jia, S. F.; Xu, B.; Worth, L, L.; Waldrep, J. C.; Fung, Y. K.; Ang, A, T.; Knight, V. *Cancer Gene Ther.* **2001**, *8*, 619–627.
(22) Smits, R. G.; Koper, G. J. M.; Mandel, M. *J. Phys. Chem.* **1993**, *97*, 5745–5751.
(23) Merdan, T.; Kunath, K.; Fischer, D.; Kopecek, J.; Kissel, T. *Pharm. Res.* **2002**, *19*, 140–146.
(24) Bieber, T.; Meissener, W.; Kostin, S.; Niemann, A.; Elsasser, H.-P. *J. Controlled Release* **2002**, *82*, 441–454.
(25) Walker, G. F.; Fella, C.; Pelisek, J.; Fahrmeir, J.; Boeckle, S.; Ogris, M.; Wagner, E. *Mol. Ther.* **2005**, *11*, 418–425.
(26) Miyata, K.; Oba, M.; Nakanishi, M.; Fukushima, S.; Yamasaki, Y.; Koyama, H.; Nishiyama, N.; Kataoka, K. *J. Am. Chem. Soc.* **2008**, *130*, 16287–16294.
(27) Moghimi, S. M.; Symonds, P.; Murray, J. C.; Hunter, A. C.; Debska, G.; Szewczk, A. *Mol. Ther.* **2005**, *11*, 990–995.
(28) Kanayama, N.; Fukushima, S.; Nishiyama, N.; Itaka, K.; Jang, W. D.; Miyata, K.; Yamasaki, Y.; Chung, U.; Kataoka, K. *ChemMedChem.* **2006**, *1*, 439–444.
(29) Itaka, K.; Ohaba, S.; Miyata, K.; Kawaguchi, H.; Nakamura, K.; Takato, T.; Chung, U.; Kataoka, K. *Mol. Ther.* **2007**, *15*, 1655–1662.
(30) Harada-Shiba, M.; Takamisawa, I.; Miyata, K.; Ishii, T.; Nishiyama, N.; Itaka, K.; Kangawa, K.; Yoshihara, F.; Asada, Y.; Hatakeyama, K.; Nagaya, N.; Kataoka, K. *Mol. Ther.* **2009**, *17*, 1180–1186.
(31) Arnida; Nishiyama, N.; Kanayama, N.; Jang, W.-D.; Yamasaki, Y.; Kataoka, K. *J. Controlled Release* **2006**, *115*, 208–215.
(32) Nakanishi, M.; Park, J.-S.; Jang, W.-D.; Oba, M.; Kataoka, K. *React. Funct. Polym.* **2007**, *67*, 1361–1372.
(33) Fisher, D.; Li, Y.; Ahlemeyer, B.; Kreglstein, J.; Kissel, T. *Biomaterials* **2003**, *24*, 1121–1131.

Journal of Controlled Release 151 (2011) 104–109

Contents lists available at ScienceDirect

Journal of Controlled Release

journal homepage: www.elsevier.com/locate/jconrel

Concept Paper

In situ quantitative monitoring of polyplexes and polyplex micelles in the blood circulation using intravital real-time confocal laser scanning microscopy

Takahiro Nomoto [a,1], Yu Matsumoto [b,c,d,1], Kanjiro Miyata [b], Makoto Oba [e], Shigeto Fukushima [f], Nobuhiro Nishiyama [b], Tatsuya Yamasoba [c], Kazunori Kataoka [a,b,f,*]

[a] *Department of Bioengineering, Graduate School of Engineering, The University of Tokyo, Japan*
[b] *Division of Clinical Biotechnology, Center for Disease Biology and Integrative Medicine, Graduate School of Medicine, The University of Tokyo, Japan*
[c] *Department of Otorhinolaryngology and Head and Neck Surgery, Graduate School of Medicine and Faculty of Medicine, The University of Tokyo, Japan*
[d] *Department of Otorhinolaryngology and Head and Neck Surgery, Mitsui Memorial Hospital, Japan*
[e] *Department of Vascular Regeneration, Division of Tissue Engineering, The University of Tokyo Hospital, Japan*
[f] *Department of Materials Engineering, Graduate School of Engineering, The University of Tokyo, Japan*

ARTICLE INFO

Article history:
Received 12 January 2011
Accepted 10 February 2011
Available online 3 March 2011

Keywords:
Intravital confocal microscopy
Polyplex
Polyethylene glycol
Block copolymer
Polymer micelle

ABSTRACT

Surface modification using poly(ethylene glycol) (PEG) is a widely used strategy to improve the biocompatibility of cationic polymer-based nonviral gene vectors (polyplexes). A novel method based on intravital real-time confocal laser scanning microscopy (IVRTCLSM) was applied to quantify the dynamic states of polyplexes in the bloodstream, thereby demonstrating the efficacy of PEGylation to prevent their agglomeration. Blood flow in the earlobe blood vessels of experimental animals was monitored in a noninvasive manner to directly observe polyplexes in the circulation. Polyplexes formed distinct aggregates immediately after intravenous injection, followed by interaction with platelets. To quantify aggregate formation and platelet interaction, the coefficient of variation and Pearson's correlation coefficient were adopted. In contrast, polyplex micelles prepared through self-assembly of plasmid DNA with PEG-based block catiomers had dense PEG palisades, revealing no formation of aggregates without visible interaction with platelets during circulation. This is the first report of *in situ* monitoring and quantification of the availability of PEGylation to prevent polyplexes from agglomeration over time in the blood circulation. This shows the high utility of IVRTCLSM in drug and gene delivery research.

1. Concept of new methodologies

Gene therapy offers a unique potential for the treatment of genetic and intractable diseases and for tissue engineering. Its success is dependent upon the development of useful gene vectors as well as application of a drug delivery system (DDS). Nonviral gene vectors are attractive alternatives to viral gene vectors because they are much simpler to produce, transport and store, and induce fewer immune responses. Cationic polymers that electrostatically interact with plasmid DNA (pDNA) have been widely studied as materials to construct nonviral gene vectors [1–5]. The cationic polymers most commonly used as gene vectors include branched polyethylenimine (BPEI), linear polyethylenimine, poly(L-lysine) (PLys), chitosan, and dendrimers [6]. These polymers form polyion complexes (polyplexes) with pDNA to successfully transfer it into cultured cells to induce appreciable level of gene expression. However, these polyplexes have biocompatibility problems for systemic application. Polyplexes usually require excess polycations to generate electrostatic repulsion for their increased solubility and colloidal stability. This eventually results in a shift of their surface charge to a positive value. This positive charge causes nonspecific interaction with anionic components in the body such as plasma proteins and blood cells, which might lead to severe adverse effects [7,8]. Attachment of hydrophilic polymers such as poly(ethylene glycol) (PEG) is called "PEGylation" and has often been used to shield nonviral gene vectors from undesired interaction in the blood. PEGylation also contributes to diminished uptake by the reticuloendothelial system or macrophages, and hence the half-life in blood circulation can be extended.

It is well documented that a PEG palisade prevents nonspecific interaction with biological components. However, *in situ* evaluation of

Abbreviations: PEG, poly(ethylene glycol); DDS, drug delivery system; pDNA, plasmid DNA; BPEI, branched polyethylenimine; PLys, poly(L-lysine); PEG-PLys, poly(ethylene glycol)-*b*-poly(L-lysine); PAsp(DET), poly{*N*-[*N*-(2-aminoethyl)-2-aminoethyl]aspartamide}; PEG-PAsp(DET), poly(ethylene glycol)-*b*-poly{*N*-[*N*-(2-aminoethyl)-2-aminoethyl] aspartamide}; IVRTCLSM, intravital real-time confocal laser scanning microscopy; CV, coefficient of variation; PCC, Pearson's correlation coefficient.

* Corresponding author at: Department of Materials Engineering, Graduate School of Engineering, The University of Tokyo, 7-3-1 Hongo, Bunkyo-ku, Tokyo 113-0033, Japan. Tel.: +81 3 5841 7138; fax: +81 3 5841 7139.
E-mail address: kataoka@bmw.t.u-tokyo.ac.jp (K. Kataoka).

[1] These authors equally contributed to this work.

0168-3659/$ – see front matter © 2011 Elsevier B.V. All rights reserved.
doi:10.1016/j.jconrel.2011.02.011

the interaction between nonviral gene vectors and biological components has not been reported due to the absence of methodology to quantify the interaction. We recently described a method of direct and instantaneous observation of intravenously injected substances using intravital real-time confocal laser scanning microscopy (IVRTCLSM) [9]. IVRTCLSM provides high-speed scanning and simultaneous capture of multicolor fluorescence. The macromolecular agents flowing in the bloodstream in tumors, kidneys, and livers can be monitored using IVRTCLSM.

In the present study, we applied IVRTCLSM for the investigation of the interaction between nonviral gene vectors and biological components *in situ*. For the PEGylated polyplexes, we focused on polyplex micelles made through the self-assembly of pDNA with PEG-based cationic block copolymers [10–12]. We further developed an analytical methodology to quantify the dynamic states of nonviral gene vectors circulating in the bloodstream. This is the first report visualizing and quantifying the interaction between nonviral gene vectors and biological components over time and in real-time *in situ*.

2. Experimental methods

2.1. Sample preparation

Sterile Hepes (1 M, pH 7.3) was purchased from Amresco (Solon, OH, USA) and used as a buffer solution after dilution with distilled water. pDNA encoding the soluble form of vascular endothelial growth factor receptor-1 was labeled with Cy5 using Label IT Tracker Nucleic Acid Localization Kits (Mirus Bio Corporation, Madison, WI, USA). BPEI (molecular weight (MW) 22 kDa; Sigma-Aldrich, St. Louis, MO, USA) was dialyzed in 0.01 M HCl and lyophilized as a hydrochloride salt. BPEI and PLys (hydrobromide salt, MW 4–15 kDa; Sigma-Aldrich) were mixed with Cy5-labeled pDNA (150 μg/mL) at an N/P ratio of 6 and 2, respectively, to form polyplexes. The N/P ratio was defined as the residual molar ratio of amino groups of cationic segment to phosphate groups of pDNA. Poly{*N*-[*N*-(2-aminoethyl)-2-aminoethyl]aspartamide} (PAsp(DET)) (polymerization degree: 95) was synthesized as described previously [13]. PAsp(DET) was mixed with Cy5-labeled pDNA at an N/P ratio of 4. Poly(ethylene glycol)-*b*-poly(L-lysine) (PEG-PLys; MW of PEG: 12,000; polymerization degree of PLys segment: 45) was synthesized as described previously [14]. Poly(ethylene glycol)-*b*-poly{*N*-[*N*-(2-aminoethyl)-2-aminoethyl]aspartamide} (PEG-PAsp(DET); MW of PEG: 12,000 Da; polymerization degree of PAsp(DET) segment: 93) was synthesized by the aminolysis of PEG-poly(β-benzyl L-aspartate) block copolymer with diethylenetriamine according to a previous report [13]. PEG-PLys/pDNA and PEG-PAsp(DET)/pDNA micelles were prepared at an N/P ratio of 2 and 4, respectively. The final Cy5-labeled pDNA concentration was adjusted to 100 μg/mL in 10 mM Hepes buffer (pH 7.3).

2.2. Animal preparation

All animal experimental procedures were executed in accordance with the Guide for the Care and Use of Laboratory Animals as stated by the National Institutes of Health. Balb/c nude mice (female; Charles River Laboratories, Tokyo, Japan) were anesthetized with 3.0%–4.0% isoflurane (Abbott Japan Co., Ltd., Tokyo, Japan) using a Univenter 400 Anaesthesia Unit (Univentor Ltd., Zejtun, Malta). Mice were then subjected to lateral tail vein catheterization with a 30-gauge needle (Dentronics Co., Ltd., Tokyo, Japan) connected to a nontoxic, medical grade polyethylene tube (Natsume Seisakusho Co., Ltd., Tokyo, Japan). Platelets were labeled *in vivo* with the intravenous injection of DyLight 488-conjugated anti-GPIbβ antibody (X488; EMFRET Analytics, Eibelstadt, Germany) following the manufacturer's instructions. Mice were placed onto a custom-designed temperature-controlled microscope stage. The ear lobe was attached beneath the cover slip with a single drop of immersion oil as described in our previous report [9]. Video acquisition of the dermis tissue at a speed of 30 frames per second was performed for 10 min. Two-hundred microliters of naked pDNA, polyplexes, and micelles (20 μg of pDNA) were administered via the tail vein catheter 10 s after video acquisition was initiated. For the platelet inhibition study, 300 μL of aspirin (acetylsalicylic acid; Sigma-Aldrich) saturated aqueous solution was orally administered to mice for 2 consecutive days before IVRTCLSM.

2.3. IVRTCLSM imaging and processing

All picture/movie acquisitions were performed using a Nikon A1R confocal laser scanning microscope system attached to an upright ECLIPSE FN1 machine equipped with a CFI Apo 40× WI λS objective lens (Nikon, Tokyo, Japan). All pictures/movies were acquired at a scale of 79.55 μm × 79.55 μm with 5.11 μm of confocal slice. Acquired data were further processed using Nikon NIS Elements software. The region of interest (ROI) was manually defined in the vein. Image frames were extracted every 5 s from the video data for further analyses. For quantification of aggregates, the coefficient of variation (CV) of Cy5 fluorescence was calculated. For the platelet interaction study, colocalization between DyLight and Cy5 was evaluated by Pearson's correlation coefficient (PCC) [15]. All obtained values were plotted against time.

3. Discovery

3.1. Real-time observation of aggregates

We prepared BPEI/pDNA (N/P = 6), PLys/pDNA (N/P = 2), and PAsp (DET)/pDNA (N/P = 4) polyplexes as well as PEG-PLys/pDNA (N/P = 2) and PEG-PAsp(DET)/pDNA (N/P = 4) micelles. BPEI/pDNA was used as the representative polyplex containing excessive polycations. N/P ratios of PLys/pDNA and PAsp(DET)/pDNA were determined as the critical ratio to condense pDNA according to our previous report [16]. N/P ratios of PEG-PLys/pDNA and PEG-PAsp(DET)/pDNA micelles were determined at the same N/P ratios of PLys/pDNA and PAsp(DET)/pDNA polyplexes, respectively. The size and zeta potentials of these polyplexes and polyplex micelles were summarized in Supplementary Table 1.

Intravenously injected polyplexes and micelles were directly observed by IVRTCLSM. These dynamic states in the bloodstream were compared (Supplementary Videos 1–5). Extracted movie frames at indicated time points are shown in Fig. 1. Immediately after the BPEI/pDNA polyplex was injected, the fluorescence of Cy5 agglomerated into clumps with a variable size in several micrometers range. This nonuniform fluorescence distribution of the polyplex indicated formation of aggregates. PLys/pDNA and PAsp(DET)/pDNA polyplexes showed similar aggregate formation. In contrast, the fluorescence of Cy5 showed uniform distribution when PEG-PLys/pDNA and PEG-PAsp(DET)/pDNA micelles were injected, indicating the absence of aggregates.

3.2. Quantification of aggregates

Using the mean intensity of Cy5 fluorescence, the amount of Cy5-labeled pDNA was evaluated. We acquired the images every 5 s, calculated the relative fluorescence intensity defined as (Cy5 mean fluorescence intensity - Cy5 minimum fluorescence intensity)/(Cy5 maximum fluorescence intensity − Cy5 minimum fluorescence intensity), and plotted the relative fluorescence intensities against time. (Supplementary Fig. 1) The relative fluorescence intensities of naked pDNA decreased immediately, and almost disappeared within 5 min after the start of acquisition. The relative fluorescence intensities of BPEI/pDNA, PLys/pDNA, and PAsp(DET)/pDNA polyplexes also rapidly decreased and dropped to around 0.2 within 10 min after the start of acquisition. In contrast, PEG-PLys/pDNA, and PEG-PAsp(DET)/pDNA polyplex micelles maintained the relative

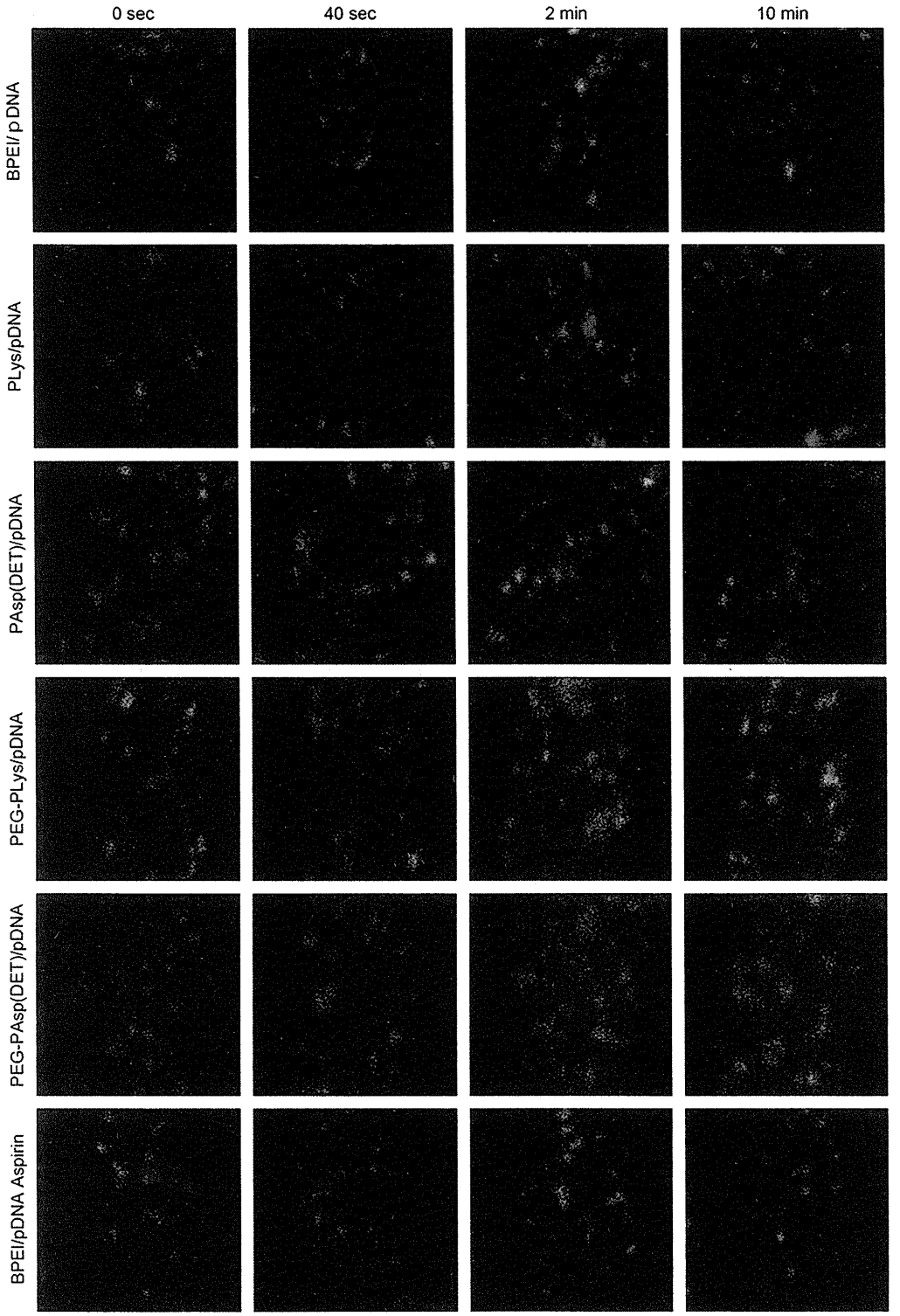

Fig. 1. Intravital confocal micro-videography of polyplexes and polyplex micelles in the bloodstream of the mouse earlobe. Prior to observation, the anti-GPIbβ antibody conjugated with DyLight 488 was injected to label platelets (green). The polyplexes and polyplex micelles incorporating Cy5-labeled pDNA (red) were intravenously injected 10 s after start of observation. Image frames were extracted from videos at identical time points for comparison. Image size: 79.55 μm × 79.55 μm. Confocal slice: 5.11 μm.

fluorescence intensities of around 0.9 and 0.7 even 10 min after the start of acquisition, suggesting the prolonged blood circulation. These results are consistent with the previous studies, which demonstrated pDNA degradation within 5 min and the improvement of blood circulation by PEGylation [17,18].

However, the relative fluorescence intensities could not provide the information about the aggregates of polyplexes and polyplex micelles. Thus, the quantification of aggregates was performed by CV calculation of Cy5 fluorescence in the ROI. The CV is a normalized measure of dispersion of a distribution, and is defined as the ratio of

the standard deviation to the mean. We acquired the images every 5 s, calculated the CV, and plotted the CV against time (Fig. 2). CV values of the polyplexes rapidly increased upon first entry into the vein of the earlobe immediately after intravenous injection. CV values of the polyplexes subsequently fluctuated and decreased over time. In contrast, CV values of the micelles slightly increased upon first entry due to the admixture of micelles and blood, and remained at a plateau at the lower values without fluctuation.

3.3. Platelet interaction study

Platelet is known to be the primary cell components involved in the initial event of thrombosis, and polycations initiate the process of platelet clots formation [19–21]. Thus, in this study, we focused on platelets interaction with cationic polyplexes. To investigate the interaction of polyplexes with platelets, we labeled platelets with DyLight 488-conjugated anti-GPIbβ antibody, and observed the interaction using IVRTCLSM (Fig. 1, Supplementary Videos 1–5). The average labeling efficiency of the antibody has been reported to be ~90% [22]. BPEI/pDNA, PLys/pDNA, and PAsp(DET)/pDNA polyplexes formed aggregates immediately after injection as described above. Their adhesion to platelets was clearly observed approximately 2 min after injection as judged from the colocalization of red and green fluorescences to appear as yellow colored pixels. In contrast, PEG-PLys/pDNA and PEG-PAsp(DET)/pDNA micelles showed no adhesion to platelets throughout the whole experiment.

3.4. Platelet interaction quantification

To quantify the interaction between polyplexes and platelets, we acquired the images every 5 s, and calculated the colocalization between Cy5 fluorescence and DyLight 488 fluorescence using PCC [15]. PCC indicates the intensity of the correlation of two elements, ranging from −1 to +1. The PCC value of the BPEI/pDNA polyplex fluctuated and increased up to approximately 0.4 (Fig. 3). PLys/pDNA and PAsp(DET)/pDNA polyplexes also fluctuated and increased up to approximately 0.25 and 0.33, respectively. In contrast, PCC values of PEG-PLys/pDNA and PEG-PAsp(DET)/pDNA micelles were maintained at almost zero throughout the study.

3.5. Platelet inhibition study

To investigate whether inhibition of platelet function decreases aggregates formation, aspirin was used as an anti-platelet agent. We compared the CV and PCC of the BPEI/pDNA polyplex between aspirin-administered mice and nonadministered control mice (Figs. 1 and 4, Supplementary Video 6). The CV value of the aspirin-administered mice was almost identical to that of control mice; however, their PCC value remained <0.1 throughout the study.

4. Interpretation and significance of new methodologies

Pharmacokinetic studies are indispensable for developing efficient DDSs that transport drugs specifically to the targeted tissue. Pharmacokinetic studies using animals have primarily relied on *ex vivo* techniques, such as analyzing blood or urine samples. These *ex vivo* techniques have been well established to analyze blood circulation, target accumulation, or other pharmacological information of the DDS. However, this approach provides only static information at specific time points. Therefore, investigating dynamic and longitudinal events using this approach is difficult. Alternatively, the intravital microscopy is an emerging technique [23], allowing to investigate such dynamic states of DDS in animals. Recently, we developed the intravital microscopy equipped with fast-scanning laser confocal systems (IVRTCLSM) [9], and demonstrated here its application as a novel tool to dynamically evaluate the interaction between gene vectors and blood components. Our method is characterized by noninvasive observation with high spatial and temporal resolutions to quantitatively monitor the dynamic states

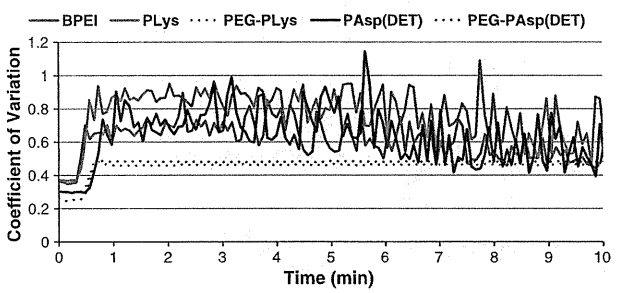

Fig. 2. Quantification of aggregates of polyplexes and micelles. Aggregates of polyplexes and micelles were quantified with CV of Cy5 fluorescence intensities in the frames extracted every 5 s from crude videos.

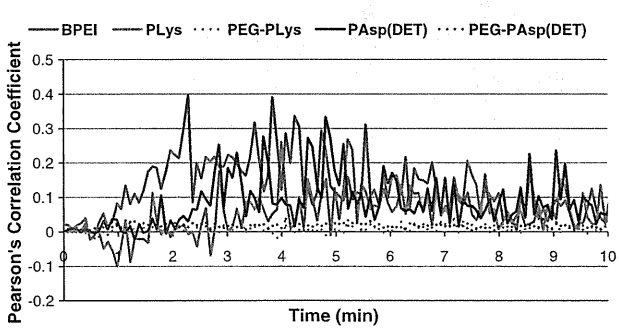

Fig. 3. Quantification of colocalization between polyplexes/micelles and platelets. The colocalization was measured with PCC. PCC was calculated from the frames extracted every 5 s from crude videos.

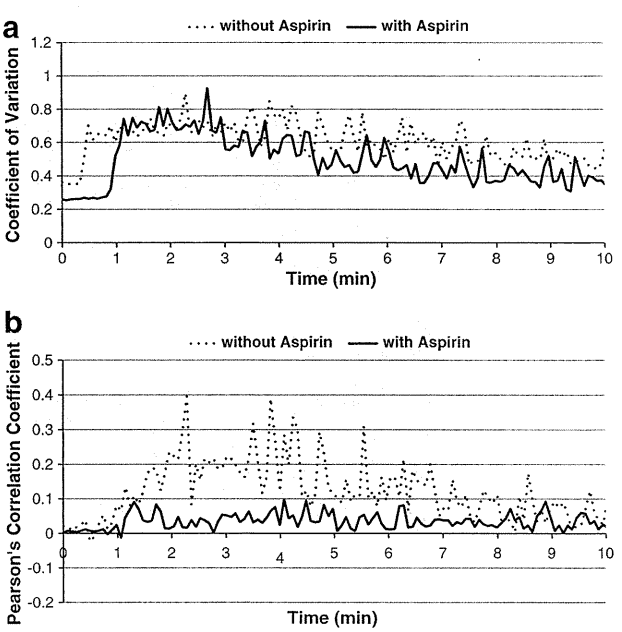

Fig. 4. Platelets inhibition study with aspirin. (a) Aggregates of BPEI/pDNA polyplexes of the aspirin-administered mouse was quantified with the CV of Cy5 fluorescence intensities in the frames extracted every 5 s from crude videos. (b) Colocalization between BPEI/pDNA polyplexes and platelets of the aspirin-administered mouse was quantified with PCC. PCC was calculated from the frames extracted every 5 s from crude videos. For comparison, the CV and PCC of the BPEI/pDNA polyplexes-administered normal mouse in Figs. 2 and 3 were shown respectively again.

of nonviral gene vectors. In the present study, the mouse earlobe was noninvasively fixed beneath the coverslip, and the vein was imaged at the dermis layer. Confocal imaging eliminated light from out-of-focus sections in the ear lobe such as the epidermis and hypodermis. Furthermore, we kept the confocal slice thinner (5.11 μm) than the diameter of the vein, so that the signal was detected only from inside the vasculature. High-speed scanning was essential to obtain unambiguous images to quantify the aggregates and colocalization between nonviral gene vectors and platelets because conventional galvano scanners are too slow to distinguish the individual aggregates and platelets rapidly flowing in the bloodstream, providing insufficient and blurred images (Supplementary Videos 7 and 8).

We investigated the polycations BPEI and PLys. They are widely used to construct polyplexes and PAsp(DET) has reduced cytotoxicity and high transfection efficiency [13]. To evaluate the improvement of biocompatibility via PEGylation, PEG-PLys/pDNA and PEG-PAsp (DET)/pDNA micelles were examined. A simple and effective way to PEGylate polyplexes is, as we reported [10–12], to use PEG-based cationic block copolymers as counterpart polycations to pDNA. The block copolymers are characterized by tandem alignment of a hydrophilic PEG segment and a cationic segment, leading to the formation of stable and biocompatible micelles with a core of polycation/pDNA complex surrounded by a dense PEG palisade and size of approximately 100 nm. Indeed, the micelle composed of PEG-PLys and pDNA achieved higher stability than that of unmodified PLys/pDNA polyplex in a medium containing serum and showed prolonged blood circulation [18,24]. The block copolymer possessing a cationic polyaspartamide segment carrying an ethylenediamine unit at the side chain, PEG-PAsp(DET), also formed the micelle with pDNA, which prevented nonspecific interaction with biological components such as erythrocytes and platelets under *in vitro* conditions [8].

IVRTCLSM was used to directly investigate the interaction between these gene vectors and platelets in the bloodstream. IVRTCLSM could be used to evaluate the dynamic states of nonviral gene vectors rapidly flowing in the bloodstream over time *in situ* (Fig. 1 and Supplementary Videos 1–6). This is the first report to visualize the formation of aggregates and the prevention by PEGlyation of polyplexes *in situ* in the bloodstream.

To quantify the aggregates, we adopted the CV. CV values reflected the nonuniform fluorescence distribution of polyplexes and uniform fluorescence distribution of micelles (Fig. 2). It is noteworthy that our IVRTCLSM started video acquisition 10 s before administration, allowing us to follow aggregate formation immediately after injection. CV values of the polyplexes rapidly increased approximately 20–30 s after injection, and corresponded well with the entry of polyplexes, indicating instantaneous formation of aggregates (Fig. 2). CV values also fluctuated over time, depending on the amount of aggregates at those time points. Furthermore, CV values of polyplexes decreased with time due to their disappearance from the bloodstream. In contrast, CV values of micelles were moderately elevated when micelles passed the ROI first. This moderate elevation was because of the admixture of micelles and blood without aggregate formation. Moreover, CV values were retained at a plateau after this moderate elevation, suggesting persistent circulation and uniform distribution of micelles in the bloodstream.

IVRTCLSM was also useful for the investigation of the dynamic interaction between nonviral gene vectors and platelets. Indeed, we succeeded in visualizing the interaction between polyplexes and platelets *in situ*. This dynamic information could not be revealed without IVRTCLSM.

To quantify the platelet interaction, we adopted PCC between polyplexes/micelles and platelets (Fig. 3). PCC values of polyplexes did not increase at the time point when CV values started to increase. PCC values began to increase after approximately 1 min after injection, and indicated strong correlation between polyplexes and platelets 2 min after injection. This temporal gap between aggregate formation and platelet interaction strongly indicated that aggregate formation was not triggered by platelets. To confirm this, we conducted the study in mice that were administered aspirin (Fig. 4). Aspirin induces a long-lasting functional defect in platelets [25], and thus may inhibit platelet interaction with polyplexes. The CV and PCC quantitatively demonstrated that oral administration of aspirin successfully inhibited platelet interaction with aggregates (Fig. 4b), but did not inhibit aggregate formation itself (Fig. 4a). This result indicates that the aggregate formation of polyplexes does not involve platelets (at least in the initial stage). Presumably, some protein components in plasma may have a role in aggregate formation, but further investigation is needed to clarify the mechanism.

Aggregate formation in the range of several micrometers immediately after intravenous injection should crucially affect the efficiency of systemically injected polyplexes. The aggregated polyplexes cannot extravasate into the targeted tissues or cells. Moreover, they might lead to thrombosis through the interaction with platelets to obstruct microvessels in normal tissue, including the lungs and liver, resulting in nonspecific accumulation of polyplexes in these tissues. This accumulation caused by aggregate formation will lead to unfavorable effects such as pulmonary embolism. The micelles, in contrast, did not form aggregates, and also showed no interaction with platelets. Thus, they are expected to prevent adverse effects caused by polyplex agglomeration, which cannot be inhibited even by oral administration of aspirin. This result confirms that PEGylation is a rational strategy to improve the biocompatibility of nonviral gene vectors based on polyplex formation [3,10–12].

In the present study, IVRTCLSM was used to visualize and quantify the dynamic states of polyplexes flowing in the bloodstream. Moreover, with respect to ethics, IVRTCLSM excels conventional *ex vivo* methods that involve the sacrifices of numerous animals to acquire pharmacokinetic information. IVRTCLSM provides temporal and spatial information at 30 time points in 1 s with a single mouse, which is desirable for high-throughput screening of newly developed DDSs.

In conclusion, IVRTCLSM was developed and applied to directly investigate the dynamic state of gene vectors in the bloodstream. Aggregate formation of the polyplexes and its prevention by PEGylation was observed *in situ* for the first time under the flow in the capillary. Thus, IVRTCLSM could provide the requisite information that has not been obtained by conventional methods, thereby giving a new facet in the research on systemic gene delivery.

Supplementary materials related to this article can be found online at doi:10.1016/j.jconrel.2011.02.011.

Acknowledgment

This work was supported in part by Core Research Program for Evolutional Science and Technology (CREST) from the Japan Science and Technology Corporation (JST) and Funding Program for World-Leading Innovative R&D on Science and Technology (FIRST Program) from Japan Society for the Promotion of Science (JSPS).

References

[1] D.W. Pack, A.S. Hoffman, S. Pun, P.S. Stayton, Design and development of polymers for gene delivery, Nat. Rev. Drug Discov. 4 (2005) 581–593.
[2] T. Merdan, K. Kunath, H. Petersen, U. Bakowsky, K.H. Voigt, J. Kopecek, T. Kissel, PEGylation of poly(ethylene imine) affects stability of complexes with plasmid DNA under in vivo conditions in a dose-dependent manner after intravenous injection into mice, Bioconjug. Chem. 16 (2005) 785–792.
[3] M. Ogris, E. Wagner, Targeting tumors with non-viral gene delivery systems, Drug Discov. Today 7 (2002) 479–485.
[4] Y. Kakizawa, K. Kataoka, Block copolymer micelles for delivery of gene and related compounds, Adv Drug Deliver Rev 54 (2002) 203–222.

[5] K. Osada, R.J. Christie, K. Kataoka, Polymeric micelles from poly(ethylene glycol)-poly(amino acid) block copolymer for drug and gene delivery, J. R. Soc. Interface 6 (2009) S325–S339.
[6] Y.Y. Yang, Y. Wang, R. Powell, P. Chan, Polymeric core–shell nanoparticles for therapeutics, Clin. Exp. Pharmacol. Physiol. 33 (2006) 557–562.
[7] M. Ogris, S. Brunner, S. Schuller, R. Kircheis, E. Wagner, PEGylated DNA/transferrin-PEI complexes: reduced interaction with blood components, extended circulation in blood and potential for systemic gene delivery, Gene Ther. 6 (1999) 595–605.
[8] D. Akagi, M. Oba, H. Koyama, N. Nishiyama, S. Fukushima, T. Miyata, H. Nagawa, K. Kataoka, Biocompatible micellar nanovectors achieve efficient gene transfer to vascular lesions without cytotoxicity and thrombus formation, Gene Ther. 14 (2007) 1029–1038.
[9] Y. Matsumoto, T. Nomoto, H. Cabral, Y. Matsumoto, S. Watanabe, R.J. Christie, K. Miyata, M. Oba, T. Ogura, Y. Yamasaki, N. Nishiyama, T. Yamasoba, K. Kataoka, Direct and instantaneous observation of intravenously injected substances using intravital confocal micro-videography, Biomed. Opt. Express 1 (2010) 1209–1216.
[10] K. Osada, R.J. Christie, K. Kataoka, Polymeric micelles from poly(ethylene glycol)-poly(amino acid) block copolymer for drug and gene delivery, J. R. Soc. Interface 6 (Suppl. 3) (2009) S325–339.
[11] Y. Kakizawa, K. Kataoka, Block copolymer micelles for delivery of gene and related compounds, Adv. Drug Deliv. Rev. 54 (2002) 203–222.
[12] N. Nishiyama, K. Kataoka, Current state, achievements, and future prospects of polymeric micelles as nanocarriers for drug and gene delivery, Pharmacol. Ther. 112 (2006) 630–648.
[13] K. Itaka, T. Ishii, Y. Hasegawa, K. Kataoka, Biodegradable polyamino acid-based polycations as safe and effective gene carrier minimizing cumulative toxicity, Biomaterials 31 (2010) 3707–3714.
[14] A. Harada, K. Kataoka, Formation of polyion complex micelles in an aqueous milieu from a pair of oppositely-charged block-copolymers with poly(ethylene glycol) segments, Macromolecules 28 (1995) 5294–5299.
[15] V. Zinchuk, O. Zinchuk, T. Okada, Quantitative colocalization analysis of multicolor confocal immunofluorescence microscopy images: pushing pixels to explore biological phenomena, Acta Histochem. Et Cytochem. 40 (2007) 101–111.
[16] K. Miyata, S. Fukushima, N. Nishiyama, Y. Yamasaki, K. Kataoka, PEG-based block catiomers possessing DNA anchoring and endosomal escaping functions to form polyplex micelles with improved stability and high transfection efficacy, J. Control. Release 122 (2007) 252–260.
[17] K. Kawabata, Y. Takakura, M. Hashida, The fate of plasmid dna after intravenous-injection in mice — involvement of scavenger receptors in its hepatic-uptake, Pharm. Res. 12 (1995) 825–830.
[18] M. Harada-Shiba, K. Yamauchi, A. Harada, I. Takamisawa, K. Shimokado, K. Kataoka, Polyion complex micelles as vectors in gene therapy — pharmacokinetics and in vivo gene transfer, Gene Ther. 9 (2002) 407–414.
[19] K. Kataoka, T. Tsuruta, T. Akaike, Y. Sakurai, Biomedical behavior of synthetic polyion complexes toward blood-platelets, Makromolekulare Chem. Macromol. Chem. Phys. 181 (1980) 1363–1373.
[20] T.K. Rosborough, Parallel inhibition of ristocetin and polycation-induced platelet agglutination, Thromb. Res. 19 (1980) 417–422.
[21] P. Chollet, M.C. Favrot, A. Hurbin, J.L. Coll, Side-effects of a systemic injection of linear polyethylenimine–DNA complexes, J. Gene Med. 4 (2002) 84–91.
[22] M.R. Dowling, E.C. Josefsson, K.J. Henley, P.D. Hodgkin, B.T. Kile, Platelet senescence is regulated by an internal timer, not damage inflicted by hits, Blood 116 (2010) 1776–1778.
[23] S. Hak, N.K. Reitan, O. Haraldseth, C. Lange Davies, Intravital microscopy in window chambers: a unique tool to study tumor angiogenesis and delivery of nanoparticles, Angiogenesis 13 (2010) 113–130.
[24] K. Itaka, K. Yamauchi, A. Harada, K. Nakamura, H. Kawaguchi, K. Kataoka, Polyion complex micelles from plasmid DNA and poly(ethylene glycol)-poly(L-lysine) block copolymer as serum-tolerable polyplex system: physicochemical properties of micelles relevant to gene transfection efficiency, Biomaterials 24 (2003) 4495–4506.
[25] C. Patrono, Aspirin as an antiplatelet drug, N. Engl. J. Med. 330 (1994) 1287–1294.

Molecular Genetics and Metabolism 102 (2011) 343–348

Contents lists available at ScienceDirect

Molecular Genetics and Metabolism

journal homepage: www.elsevier.com/locate/ymgme

Clinical and molecular investigation of 19 Japanese cases of glutaric acidemia type 1

Yuichi Mushimoto *, Seiji Fukuda, Yuki Hasegawa, Hironori Kobayashi, Jamiyan Purevsuren, Hong Li, Takeshi Taketani, Seiji Yamaguchi

Department of Pediatrics, Shimane University Faculty of Medicine, Shimane, Japan

ARTICLE INFO

Article history:
Received 10 September 2010
Received in revised form 12 November 2010
Accepted 14 November 2010
Available online 25 November 2010

Keywords:
Glutaric acidemia type 1 (GA1)
Glutaryl-CoA dehydrogenase (GCDH)
Organic acidemia
Genotype-phenotype correlation
Common mutation

ABSTRACT

Glutaric acidemia type 1 (GA1) is a metabolic disease caused by a deficiency of glutaryl-CoA dehydrogenase (GCDH). Untreated patients mostly develop severe striatal degeneration. More than 200 mutations have been reported in the *GCDH* gene, and common R402W and IVS10-2A>C were found in Caucasian and Chinese/Taiwanese, respectively. However, in Japan, genetic mutations have only been reported in a few cases. Herein, we report the clinical and molecular basis of GA1 in 19 Japanese patients, including six previously reported patients. All cases showed high urinary glutaric acid excretion. Eleven patients were severely impaired (three patients died), three had mild impairment, and five showed normal development. Four of 5 patients that developed normally were detected in the presymptomatic stage by neonatal or sibling screening. Nineteen mutations in 26 alleles were identified, and eight of them (89 or 90delC, Y155C, IVS4+2T C, G244S, Q352X, G354A, K361E, and 1144-1145delGC) were novel. S305L (12.1%, 4/34 alleles) was found in several cases, suggesting that this mutation is a common mutation. In contrast, R402W was not identified and IVS10-2A>C was only found in one allele, suggesting that Japanese patients with GA1 show allelic heterogeneity and have a different genetic background to patients from other countries. One of a pair of sisters with the same mutations (M339V/S305L) lacking residual activity was severely retarded, whereas the older girl remains asymptomatic at 22 years of age, indicating that genotype does not necessarily predict GA1 phenotype. We consistently found that there was no association between genotype and phenotype. However, children with mild impairment were diagnosed and treated earlier than severely impaired cases {4.7±2.5 months (range: 2–8 months) vs. 11.6±12.7 months (range: 4–51 months)}. Our results suggest that early detection and treatment but not genotype are associated with better patient outcome, reinforcing the importance of neonatal screening.

1. Introduction

Glutaric aciduria type 1 (GA1, OMIN 231670) is an autosomal recessive metabolic disorder caused by deficiency of glutaryl-CoA dehydrogenase (GCDH, EC 1.3.99.7) [1,2]. GCDH is located in the mitochondrial matrix and acts in the intermediate steps of lysine, hydroxylysine, and tryptophan metabolisms [3]. The clinical manifestations of GA1 include extrapyramidal symptoms, developmental regression, and macrocephaly, appearing most often after acute encephalopathic crises, which are accompanied by bilateral marked enlargement of the sylvian fissure and degeneration of the striatum [1], and in addition, extrastriatal abnormalities [4] and abnormal hemodynamic changes [5]. Its biochemical characteristics include the accumulation of glutaric acid (GA), and 3-hydroxyglutaric acid, which can be detected by gas chromatography (GC/MS), and glutarylcarnitine, which can be identified by electrospray ionization/tandem mass spectrometry (MS/MS) [1,2]. It has been reported that GA1 can be classified into two types based on the level of excreted GA: the high excretion form (GA>100 mmol/mol creatine) and the low excretion form (GA<100 mmol/mol creatine) [6].

Since GA1 was first described in 1975 [3], more than 200 different mutations have been reported [7–9], and its frequency was estimated to be approximately 1 in 100,000 newborns [2]. Although almost all mutations are private, several common mutations have been identified, including A421V in the Amish Community [10], IVS 1+5G T in Canadian Oji-Cree Indians [11], and E365K in Irish travelers [8]. R402W is the most frequent mutation in the European population [6,8], and IVS10-2A C is relatively common in China [12] and Taiwan [13]. In Japan, the frequency of GA1 has been estimated to be approximately 1 in 210, 000 newborns, based on a newborn screening pilot study [14,15]. However, mutations have only been characterized in a few cases [16] since the first description of a Japanese case in 1987 [17]. Herein, we investigated the clinical and molecular aspects of 19 Japanese patients with GA1.

2. Subjects and methods

2.1. Subjects

We studied 19 Japanese patients who were diagnosed with GA1 based on their urinary organic acid profiles and/or blood acylcarnitine

* Corresponding author. Department of Pediatrics, Shimane University Faculty of Medicine, 89-1 Enya, Izumo, Shimane 693-8501, Japan. Fax: +81 85 320 2215.
E-mail address: mushiu1@med.shimane-u.ac.jp (Y. Mushimoto).

1096-7192/$ – see front matter © 2010 Elsevier Inc. All rights reserved.
doi:10.1016/j.ymgme.2010.11.159

analysis. The diagnoses were confirmed by analyzing the *GCDH* gene and/or GCDH activity.

The mutations of 6 cases (cases 2–5, 12, and 19) were reported previously (cases 4, 12, and 19: [16], cases 2, 3, and 5: Japanese domestic journal). In this study, we analyzed the mutations in 13 cases (cases 1, 6–11, and 13–18). Among the 13 patients, 4 cases (case 6, 7, 10, and 11) were previously described in case reports [18,19]. No family demonstrated consanguineous marriage.

2.2. DNA sequencing

Genomic DNA was isolated from skin fibroblasts using a Qiamp DNA Microkit (QIAGEN GmbH, Hilden, Germany) and from peripheral blood lymphocytes using the DNA Quick II kit (Dainippon Pharmaceuticals, Osaka, Japan). Each exon of *GCDH* including the intron/exon boundaries was PCR-amplified for 30 cycles using the conditions shown in Supplemental Table 1. The PCR products were purified using a QIAquick PCR Purification Kit (QIAGEN GmbH, Hilden, Germany) and sequenced using the ABI PRISM 310 Genetic Analyzer (PE Applied Biosystems, Foster City, CA, USA) or the CEQ 8000 Genetic Analysis System (Beckman Coulter Inc., Fullerton, CA, USA). The structure of the human *GCDH* gene was obtained from the GenBank database (ENSG00000105607). Informed consent to perform DNA analysis was obtained from the parents of the patients. Our study protocol was approved by the Ethics Committee of the Shimane University Faculty of Medicine.

3. Results

3.1. Clinical characteristics

The clinical features of 19 Japanese GA1 patients (10 boys and 9 girls) are summarized in Table 1. Cases 4 and 19 and cases 15 and 18 were siblings. Fifteen of the 19 cases were symptomatic patients. Three (cases 1–3) of 19 cases were detected in a newborn screening pilot study, and one (case 4) was an asymptomatic sibling case that was detected at 2 years of age. To evaluate their outcomes, we classified them into three groups based on disability score [20] that included motor disability, cognitive function, and speech: a) the severe handicap group (disability score 7–9), b) the mild impairment group (disability score 4–6), and c) the normal developmental group (disability score 3) (Supplemental Table 2).

Eleven of the 19 cases were classified into severe handicap group (three of them died), 3 cases belonged to mild impairment group, and 5 cases showed normal development (Fig. 1). The mean age at onset of the symptomatic cases was 5.7 m (range: 4–8 m) in the severe handicap group, 2.3 m (range: 2–3 m) in the mild impairment group, and 6 m in case 4 of the normal development group who suffered from macrocephaly. The mean age at diagnosis was 11.6 m (range: 4–51 m) in the severe handicap group, 4.7 m (range: 2–8 m) in the mild impairment group, and 27 m (range: 24–30 m) in the normal development group, except for the 3 cases diagnosed by newborn screening. Macrocephaly was observed in 31.6% of patients (6/19). All 19 cases showed high urinary glutaric acid excretion. Cranial CT and/or MRI demonstrated frontotemporal atrophy and striatum signal abnormalities in all cases involving mild impairment or severe handicap. In contrast, three of five cases in the normal development group demonstrated mild changes by neuroimaging.

3.2. Clinical manifestations of patients

No cases had a past history except for cases 1, 6, 7, and 9. None of the cases showed abnormal development before the onset of GA1. Immediately after the diagnosis of GA1, all cases were treated with dietary restriction, L-carnitine administration, and prompt intravenous fluid infusions for catabolic states such as recurrent vomiting and diarrhea. In addition, a GABA analogue and vitamin B2 were given to the 14 and 8 cases, respectively.

3.2.1. Normal development group

Cases 1–3 were detected prior to displaying any specific symptoms by a newborn screening program using MS/MS. Case 1 weighed 2952 g when she was born at a gestational age of 39 weeks and 2 days. Abruptio placentae occurred during her birth and she suffered from asphyxia (Apgar score: 3/4). She recovered following hypothermia treatment for hypoxic–ischemic encephalopathy. Cases 2 [21] and 3 [21] had no remarkable delivery events. In these 3 cases, no signs of neurologic complications were evident at 4 months, 5 years, and 7 years old, respectively.

Case 4 was the nonsymptomatic older sister of case 19, who was severely handicapped [16]. She was diagnosed with GA1 by a sibling GC/MS screening in the presymptomatic stage at 2 years old.

Case 5 was hospitalized because of macrocephaly (47.6 cm, +2.5 S.D.) at 6 months. There was no sign of neurologic complications or developmental delay, but cranial CT suggested a subarachnoid cyst and a subdural hematoma. Thereafter, the subarachnoid cyst and subdural hematoma became smaller. At 2.5 years, he was referred to the pediatric department due to progressive macrocephaly (56.5 cm, +3.0 S.D.). Brain CT demonstrated widening of the Sylvian fissures, which in fact had been found by CT at 7 months.

3.2.2. Mild impairment group

Case 6 was treated for initial vomiting and idiopathic hyperbilirubinemia during the neonatal period [18]. Screening by brain echography identified dilated ventricles.

Case 7 was delivered at 27 weeks of dizygotic twin gestation [18]. His birth weight was 998 g. Macrocephaly and convulsions were noticed at 2 and 3 months, respectively. Following treatment, his development caught up.

In case 8, progressive macrocephaly was noticed at 3 months old. Her head circumference was +5.0 S.D. at 7 months old. Her regression and hypotonia, which were accompanied by seizures at 8 months old, improved gradually after treatment.

3.2.3. Severe handicap group

Cases 10, 11, and 13 died. Case 10 displayed a lack of head control at 4 months old [17,18] and irritability and sleeplessness at 5 months old. She died suddenly at 5 years old after developing a common cold. Cases 11 [19] and 13 presented encephalitis-like disease at 5 and 7 months, respectively. Case 11 died suddenly at the age of 3 years. Case 13 died of airway obstruction due to choking after developing an infection at 3 years old.

Similarly, no treatment was effective for the neurological symptoms of the severely handicapped patients that survived, all of whom are bedridden, require tube feeding, and smile spontaneously. Case 9 was born at 35 weeks with an Apgar score of 6/9 by cesarean delivery for premature membrane rupture and breech presentation. His birth weight was 2235 g. He was diagnosed with GA1 at 4 months after an episode of convulsions. He required mechanical ventilation and a tracheostomy for respiratory distress at 10 months old. Case 12 suffered from encephalitis-like symptoms including convulsions, unconsciousness, and rigidity following fever and an upper respiratory tract infection at 5 months old [16]. Case 14 was affected with Kawasaki disease at 5 months old. Intravenous immunoglobulin resulted in rapid defervescence, but his regression, involuntary movement, and irritability accompanied by fever were irreversible. Case 16 was affected by viral encephalitis with hyperpyrexia, consciousness disturbance, and hypertonia at 7 months of age. Case 17 was found to have subependymal pseudocysts and temporal lobe hypoplasia at 1 month. Transient regression was observed at 7 months after gastroenteritis. Thereafter, progressive neurological regression, hypotonia, and rigidity were observed following convulsions associated with pneumonia at 8 months. Case 19 was the younger sister of

Table 1
Clinical manifestations and genetic characteristics of Japanese patients with glutaric acidemia type 1.

Case I.D	Sex	Age at onset	Age at diagnosis	Precipitating factor	Clinical symptoms	Macrocephaly	Treatment	Outcome	Urine GA	C5DC (<0.3)	Neuroimaging	Exon or intron affected	Base change	Effect	GCDH activity
Normal development group															
(Newborn screening cases)															
1	F	–	1m	None	Normal development	–	L-carnitine	Normal (4m)	High	1.08	Typical	**Exon9 / Exon10**	**1064 G>A / 1147 C>T**	**R355H/R383C**	N.D
2	F	–	1 m	None	Normal development	–	L-carnitine	Normal (5y4m)	High	2.22	Mild	Exon6 / Exon8	556 A>T / 914 C>T	S186C / S305L	Deficiency
3	F	–	1 m	None	Normal development	–	L-carnitine	Normal (7y6m)	High	1.95	Mild	Exon3 / Exon10	215 G>T / 1237 T>G	R72L /Y413D	Deficiency
(Sibling screening cases)															
a 4	F	–	2 y 0 m	None	Normal development	–	L-carnitine, GABA analogue	Normal (22y)	High	N.D	Mild	Exon8 / Exon9	914C >T / 1015A> G	S305L / M339V	Deficiency
(other cases except for screening)															
5	M	6	2 y 6 m	None	Normal development	+	L-carnitine, vitamin B2	Normal (6y11m)	High	4.4	Typical	Exon5 / ?	416C >T / ?	S139L / ?	Deficiency
Mild impairment group															
6	M	2 m	2 m	None	Enlargement of ventricles	+	L-carnitine, vitamin B2, GABA analogue	Mild (23y)	High	N.D	Typical	**Exon8 / Exon10**	**914C >T / 1147 C>T**	**S305L / R383C**	Deficiency
7	M	2 m	4 m	None	Seizure	+	L-carnitine, GABA analogue	Mild (25y)	High	N.D	Typical	**Exon5 / Exon5**	**413G>A / 416C>T**	**R138K / S139L**	Deficiency
8	F	3 m	8 m	None	Seizure, regression	+	L-carnitine, GABA analogue, antiepileptic	Mild (3y2m)	High	3.36	Typical	**Exon8/ Exon9**	**914C >T / 1081A> G**	**S305L / K361E**	N.D
Severe handicap group															
9	M	4 m	4 m	None	Seizure, regression	+	L-carnitine, vitamin B2, antiepileptic	Severe (1y4m)	High	N.D	Typical	**Intron4 / Exon6**	**IVS4+2T>C / 532G>A**	**Truncated (Splicing) / G178R**	N.D
10	F	4 m	7 m	None	Regression, irritability, sleeplessness, dystonia	–	L-carnitine, vitamin B2, GABA analogue	Severe (5y:died)	High	N.D	Typical	**Exon9 / Exon9**	**1054C > T / 1054C> T**	**Truncated(Q352stop) / Truncated(Q352stop)**	Deficiency
11	M	5 m	6 m	None	Seizure, regression, hypotonia, dystonia	–	L-carnitine, GABA analogue	Severe (3y:died)	High	N.D	Typical	**Exon3 / Exon7**	**226C>T / 730G>A**	**Truncated (Q76stop) / G244S**	Deficiency
12	M	5 m	6 m	Infection, fever	Seizure, dystonic	–	L-carnitine, vitamin B2, GABA analogue	Severe (14y6m)	High	N.D	Typical	Exon9 / Exon9	1064G >A / 1064G >A	R355H / R355H	N.D
13	F	5 m	7 m	Infection	Seizure, regression, hypertonia	–	L-carnitine, GABA analogue	Severe (3y9m: died)	High	N.D	Typical	**Exon9 / Intron10**	**1061G > C / IVS10-2 A>C**	**G354A / Truncated (splicing)**	Deficiency
14	M	5 m	7 m	Kawasaki disease	Regression, dystonia	–	L-carnitine, GABA analogue, antiepileptic	Severe (7y)	High	1.76	Typical	**Exon5 / Exon7**	**416C >T / 769C>T**	**S139L / R257W**	Deficiency
b 15	M	5 m	4 y 3 m	Fever of unknown origin	Regression, dystonia	–	L-carnitine, vitamin B2, GABA analogue	Severe (5y2m)	High	0.38	Typical	**Exon1 / Exon5**	**89 or 90delC / 461A>G**	**Truncated (frame shift) / Y155C**	N.D
16	M	7 m	7 m	Infection, fever	Unconscious, dystonia	–	L-carnitine, GABA analogue	Severe (1y1m)	High	0.57	Typical	**Exon10 / Exon11**	**1144-1145delGC / 1298C>T**	**Truncated (frame shift) / A433V**	N.D
17	M	7 m	12 m	Gastroenteritis	Seizure, regression, dystonia, hypotonia	+	L-carnitine, GABA analogue, antiepileptic	Severe (2y5m)	High	N.D	Typical	**Exon5 / Exon10**	**383G>A/ 1147C>T**	**R128Q / R383C**	Deficiency
b 18	F	8 m	9 m	Polio vaccine, infection, fever	Regression, dystonia	–	L-carnitine, vitamin B2, GABA analogue	Severe (1y8m)	High	0.41	Typical	**Exon1 / Exon5**	**89 or 90delC / 461A>G**	**Truncated (frame shift) / Y155C**	Deficiency
a 19	F	8 m	12 m	Gastroenteritis	Coma, dystonia	–	L-carnitine, vitamin B2, GABA analogue	Severe (20y)	High	N.D	Typical	Exon8 / Exon9	914C >T / 1015A>G	S305L / M339V	Deficiency

Abbreviations: a,b, siblings; M, male; F, female; Age, y (years); m (months); Treatment, except for dietary restriction ; GA, glutaric acid; C5DC, glutarylcarnitine in dried spots (nmol/ml) when the patient was diagnosed; GCDH, glutaryl-CoA dehydrogenase.
Novel mutations are underlined. The mutations highlighted in bold were identified in this study; Deficiency: GCDH activity ≤5%.
N.D: not determined.

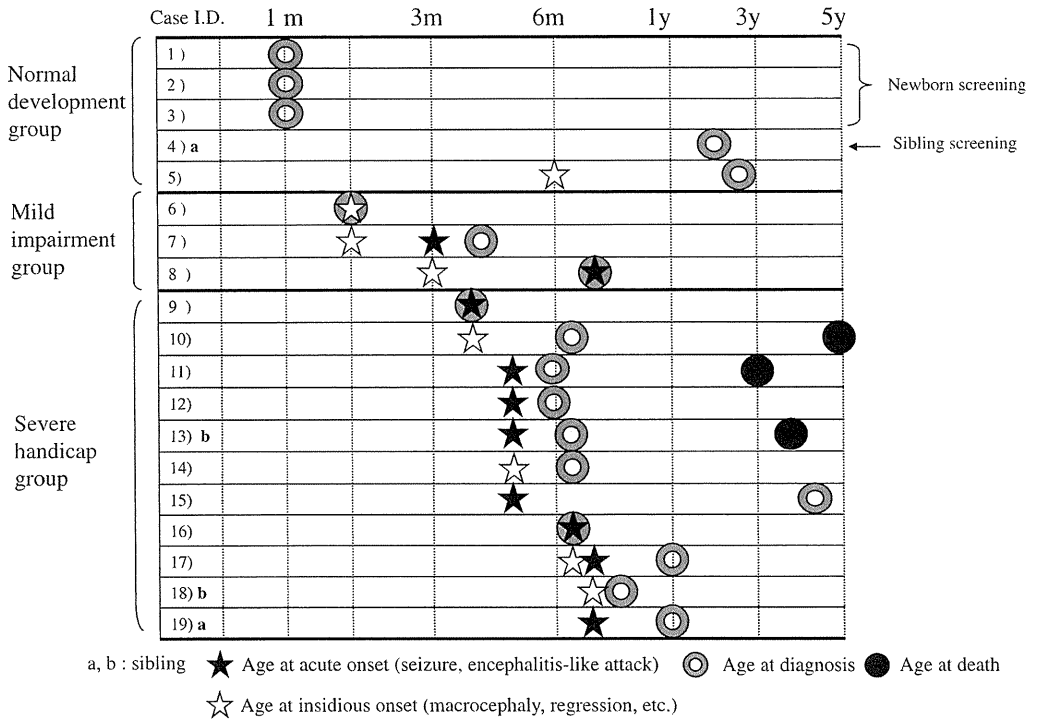

Fig. 1. Age at onset and diagnosis in three groups with different outcomes. The mild impairment group was diagnosed earlier than the severe handicap group {4.7 m (2–8 m) vs. 11.6 m (4–51 m)}. Three cases (cases 10, 11, and 13) died.

case 4. At 8 months old, she suffered an encephalopathic crisis after gastroenteritis, which lasted for several days [16]. Cases 15 and 18 were siblings. Case 15, the older brother, was hospitalized for fever of unknown origin at 5 months of age and treated with antibiotics for 10 days. In addition to hypotonia, which appeared at the time of discharge, his regression, rigidity, and involuntary movement worsened every month that he suffered from fever. Although idiopathic encephalopathy was initially suspected, a diagnosis of GA1 was made in a sibling screening program by GC/MS, and treatment was initiated at 4 years and 3 months. Case 18 suffered from fever after polio vaccination at 8 months. Thereafter, she became unable to support her head and roll over. Her neurological skills deteriorated every month that she suffered from fever. The diagnosis of GA1 was made by GC/MS at 9 months of age.

3.3. Gene mutations in GCDH

Nineteen mutations were identified in 13 cases, and 8 of them were novel. These included four missense mutations (Y155C, G244S, G354A, and K361E), a nonsense change (Q352X), a splice site alteration (IVS4+2T>C), and frame shift mutations (89 or 90delC, and 1144-1145delGC). These novel mutations were not detected in 100 chromosomes from unaffected Japanese individuals.

All mutations are summarized in Table 1 and Supplemental Fig. 1, together with information on 6 cases whose genetic alterations were reported previously ([16] and Japanese domestic journal). Only two unrelated patients out of 19 cases had homozygous mutations (Q352X, R355H). In 34 independent alleles, the frequency of S305L was 12.1% (4/34 alleles), S139L, R355H, and R383C had frequencies of 8.8% (3/34 alleles), respectively and Q352X were found in 2 alleles (5.8%) each. Another 19 mutations were only found in a single allele.

4. Discussion

Since it has been remaining unknown whether there are common mutations and a phenotype/genotype correlation in Japanese GA1 cases, we investigated the relationship between clinical and mutational spectrums of 19 Japanese patients with GA1. Japanese are relatively homogenous ethnic population on islands isolated from other countries. We found a few common mutations distinct from other nations. We also found that mutations in Japanese cases are different from what have been reported in the Caucasian cases, indicating specific genetic information unique for Japanese cases are crucial for their diagnosis in the future. The current study also indicates that earlier detection of the disease followed by appropriate medicare is crucial for the better outcome than the genotype, reinforcing the importance of neonatal screening for GA1. This is a first report that studied the largest cohort of Japanese patients with GA1.

In this study, we identified 19 mutations in 24 independent alleles including eight novel mutations. The amino acids affected by these new mutations are highly conserved among different species (Pan troglodytes, mice, Xenopus, and Bordetella parapepertusis) including humans, suggesting that the region plays an important functional role in GCDH activity. It is highly likely that Q352X, 89 or 90 delC, 1144-1145delGC, and IVS4+2T C abolish GCDH activity, because these mutations result in truncation of the peptide. G354S and Y155H, which affect the same positions as G354A and Y155C, respectively, were reported to have no enzymatic activity [6,7]. The homology of the peptide's structure indicates that G244, G354, and K361 are conserved in the acyl-CoA dehydrogenase group [22]. These findings suggested that all 8 novel mutations in this study have little GCDH activity. In the 19 Japanese cases of GA1 including 6 previously reported patients, Q352X and R355H were homozygous mutations and found in 2 alleles. The frequency of S305L was 12.1% (4/34 alleles), suggesting that this mutation is common in Japanese, in contrast to the very few reports of this mutation from other countries. S139L, R355H, and R383C were also found on 8.8% (3/34 alleles), respectively, implicating that these mutations may be also common, respectively. Additionally, mutations in exon 9 were found more frequently in Japanese GA1 compared with the report by the HGMD (http://www.hgmd.cf.ac.uk/ac/index.php). It is highly likely that understanding common mutations

will facilitate rapid and accurate diagnosis of Japanese cases with GA1. Furthermore, this information may be useful for other Asian countries as well, since some of them are shared with patients from other Asian countries. Newborn screening using MS/MS is becoming popular, and the number of patients will become larger in Asian countries [23] as well as the other countries [24–26]. R402W, the most common mutation in Caucasians, in whom it shows an allele frequency of 12–25% [6,8], was not found in our Japanese cases. IVS10-2A C, a common mutation in China (30%, 3/10 alleles) [10] and Taiwan (66.7%, 4/6 alleles) [13], was also only found in a single allele in our study. Collectively, these findings suggest that Japanese GA1 patients show allelic heterogeneity and have different genetic backgrounds to GA1 patients from other countries. However, S139L, R355H and G178R, in addition to IVS10-2A C, may be common mutations among oriental populations, since S139L have been discovered in 2 of 4 alleles in Korean cases [27], and R355H and G178R were detected in one allele in Chinese case, respectively [10].

All 19 cases demonstrated a high-excretor phenotype in urinary organic acid analysis by GC/MS, suggesting that their mutations resulted in lower enzyme activity (≤5%) [6]. In fact, an enzyme assay confirmed 0–5% residual GCDH activity in 11 cases (Cases 2–7, 10–11, 13–14, and 19) [19,21,28,29]. Furthermore, an *in vitro* probe assay using cultured fibroblasts and MS/MS demonstrated a deficiency of GCDH in 10 cases (cases 4, 6, 7, 10, 11, 13–14, and 17–19) [30]. Although all 19 cases were assumed to have barely detectable enzyme activity, their clinical outcomes were diverse, ranging from normal development, through mild impairment, to severe handicap. This study suggests that the phenotypes of Japanese GA1 patients are not associated with a specific genotype. A previous study also showed that there is no clear correlation between genotype, biochemical phenotype, and the clinical severity of GA1 [6,24]. Frequency (31.6%: 6/19 cases) of macrocephaly of this study is lower than other reports (65–75%) [2,31]. This may represent unique phenotype in Japanese patients with GA1, which have genetic backgrounds distinct from other nations. However, additional case studies are warranted to validate whether this is indeed the cases.

All symptomatic cases except for case 5 had mild impairment or severe handicap indicating that the neurological sequelae of symptomatic cases are poor in Japanese GA1 patients, as reported in previous cases [24,31–33]. With respect to the grounds for the neurological manifestation, we were not able to completely rule out hypoxic–ischemic encephalopathy, hyperbilirubinemia, prematurity, very low birth weight, or encephalitis. However, since there was no sign of neurologic complications or developmental delay before the onset in any cases, we suspect that the neurological symptoms are not a consequence of these conditions. Importantly, the mild impairment group was diagnosed earlier than the severe handicap group {4.7 ± 2.5 m (2–8 m) vs. 11.6 m ± 12.7 m (4–51 m)}, suggesting that a better outcome was induced by early diagnosis. The reason for the better outcome seen in the patients who were diagnosed younger age was considered that early diagnosis led to an earlier initiation of the treatment and/or intervention in a timely manner for any medical conditions, which in turn prevented patients from neurological impairment. The frequency of macrocephaly was higher in the mild impairment group (3/3 cases) than in the severe impairment group (2/11 cases), making it likely that macrocephaly led to an early diagnosis of GA1. Furthermore, there was a notable difference in the phenotypes of siblings with the same mutations: case 4 showed normal development, whereas case 19 showed severe retardation (Supplemental Fig. 2), indicating that genotype does not predict clinical outcome. Taken together, these findings strongly suggest that early diagnosis and treatment but not genotype are associated with a better patient outcome.

Because the diagnosis was made by newborn screening only in 15.8% (3/19 cases), there is no direct evidence that newborn screening has neuroprotective effect for the patients with GA1 in this study. However, our study indicates that genotype does not necessarily predict clinical outcome and that early diagnosis and treatment are critical for a better outcome. While indirect findings, these observations strongly suggest that earliest diagnosis by the newborn screening will also be beneficial for a better outcome. In this regard, it is very important to expand newborn screening by MS/MS to improve the outcome of Japanese GA1 patients.

Supplementary materials related to this article can be found online at doi:10.1016/j.ymgme.2010.11.159.

Acknowledgments

We thank the attending physicians in charge of the present cases for providing clinical information regarding each patient. We are also grateful to Nana Tomita, Mayumi Nagase, Mayumi Naito, Midori Furui, Rie Eda, Toyomi Esumi, Yuka Ito, and Shine Mushimoto for their technical assistance. This study was partly supported by grants from The Ministry of Health, Labor, and Welfare of Japan and from the Ministry of Education, Culture, Sports, Science, and Technology.

References

[1] F.F. Goodman SI, Organic acidemias due to defects in lysine oxidation: 2-ketoadipic academia and glutaric acidemia, in: e.a. Scriver C (Ed.), Mol Met Basis Inher Dis, McGraw-Hill Inc, New York, 2001, pp. 2195–2204.
[2] S. Kolker, E. Christensen, J.V. Leonard, C.R. Greenberg, A.B. Burlina, A.P. Burlina, M. Dixon, M. Duran, S.I. Goodman, D.M. Koeller, E. Muller, E.R. Naughten, E. Neumaier-Probst, J.G. Okun, M. Kyllerman, R.A. Surtees, B. Wilcken, G.F. Hoffmann, P. Burgard, Guideline for the diagnosis and management of glutaryl-CoA dehydrogenase deficiency (glutaric aciduria type I), J. Inherit. Metab. Dis. 30 (2007) 5–22.
[3] S.I. Goodman, S.P. Markey, P.G. Moe, B.S. Miles, C.C. Teng, Glutaric aciduria; a "new" disorder of amino acid metabolism, Biochem. Med. 12 (1975) 12–21.
[4] I. Harting, E. Neumaier-Probst, A. Seitz, E.M. Maier, B. Assmann, I. Baric, M. Troncoso, C. Muhlhausen, J. Zschocke, N.P. Boy, G.F. Hoffmann, S.F. Garbade, S. Kolker, Dynamic changes of striatal and extrastriatal abnormalities in glutaric aciduria type I, Brain 132 (2009) 1764–1782.
[5] K.A. Strauss, P. Donnelly, M. Wintermark, Cerebral haemodynamics in patients with glutaryl-coenzyme A dehydrogenase deficiency, Brain 133 (2010) 76–92.
[6] E. Christensen, A. Ribes, B. Merinero, J. Zschocke, Correlation of genotype and phenotype in glutaryl-CoA dehydrogenase deficiency, J. Inherit. Metab. Dis. 27 (2004) 861–868.
[7] S.I. Goodman, D.E. Stein, S. Schlesinger, E. Christensen, M. Schwartz, C.R. Greenberg, O.N. Elpeleg, Glutaryl-CoA dehydrogenase mutations in glutaric acidemia (type I): review and report of thirty novel mutations, Hum. Mutat. 12 (1998) 141–144.
[8] J. Zschocke, E. Quak, P. Guldberg, G.F. Hoffmann, Mutation analysis in glutaric aciduria type I, J. Med. Genet. 37 (2000) 177–181.
[9] M. Schwartz, E. Christensen, A. Superti-Furga, N.J. Brandt, The human glutaryl-CoA dehydrogenase gene: report of intronic sequences and of 13 novel mutations causing glutaric aciduria type I, Hum. Genet. 102 (1998) 452–458.
[10] B.J. Biery, D.E. Stein, D.H. Morton, S.I. Goodman, Gene structure and mutations of glutaryl-coenzyme A dehydrogenase: impaired association of enzyme subunits that is due to an A421V substitution causes glutaric acidemia type I in the Amish, Am. J. Hum. Genet. 59 (1996) 1006–1011.
[11] C.R. Greenberg, D. Reimer, R. Singal, B. Triggs-Raine, A.E. Chudley, L.A. Dilling, S. Philipps, J.C. Haworth, L.E. Seargeant, S.I. Goodman, A G-to-T transversion at the +5 position of intron 1 in the glutaryl CoA dehydrogenase gene is associated with the Island Lake variant of glutaric acidemia type I, Hum. Mol. Genet. 4 (1995) 493–495.
[12] N.L. Tang, J. Hui, L.K. Law, Y.Y. Lam, K.Y. Chan, W.L. Yeung, A.Y. Chan, K.L. Cheung, T.F. Fok, Recurrent and novel mutations of GCDH gene in Chinese glutaric acidemia type I families, Hum. Mutat. 16 (2000) 446.
[13] S.G. Shu, C.R. Tsai, L.H. Chen, C.S. Chi, Type I glutaric aciduria: phenotypes and genotypes in 5 Taiwanese children, J. Formos. Med. Assoc. 102 (2003) 729–732.
[14] Y. Shigematsu, S. Hirano, I. Hata, Y. Tanaka, M. Sudo, N. Sakura, T. Tajima, S. Yamaguchi, Newborn mass screening and selective screening using electrospray tandem mass spectrometry in Japan, J. Chromatogr. B 776 (2002) 39–48.
[15] Y. Shigematsu, I. Hata, Jpn J. Pediatr. Med. 42 (2010) 1200–1204, (in Japanese).
[16] H. Ikeda, T. Kimura, T. Ikegami, M. Kato, A. Matsunaga, S. Yokoyama, S. Yamaguchi, T. Ohura, K. Hayasaka, Novel mutations of the glutaryl-CoA dehydrogenase gene in two Japanese patients with glutaric aciduria type I, Am. J. Med. Genet. 80 (1998) 327–329.
[17] S. Yamaguchi, T. Orii, K. Yasuda, Y. Kohno, A case of glutaric aciduria type I with unique abnormalities in the cerebral CT findings, Tohoku J. Exp. Med. 151 (1987) 293–299.
[18] H. Nagasawa, S. Yamaguchi, Y. Suzuki, M. Kobayashi, Y. Wada, K. Shikura, S. Shimao, T. Okada, T. Orii, Neuroradiological findings in glutaric aciduria type I: report of four Japanese patients, Acta Paediatr. Jpn 34 (1992) 409–415, (Overseas edition).
[19] H. Osaka, S. Kimura, A. Nezu, S. Yamazaki, K. Saitoh, S. Yamaguchi, Chronic subdural hematoma, as an initial manifestation of glutaric aciduria type-1, Brain Dev. 15 (1993) 125–127.
[20] M. Kyllerman, O. Skjeldal, E. Christensen, G. Hagberg, E. Holme, T. Lonnquist, L. Skov, T. Rotwelt, U. von Dobeln, Long-term follow-up, neurological outcome and survival rate in 28 Nordic patients with glutaric aciduria type 1, Eur. J. Paediatr. Neurol. 8 (2004) 121–129.
[21] Y. Shigematsu, I. Hata, Y. Tanaka, G. Tajima, N. Sakura, E. Naito, T. Yorifuji, Stable-isotope dilution gas chromatography-mass spectrometric measurement of 3-hydroxyglutaric

acid, glutaric acid and related metabolites in body fluids of patients with glutaric aciduria type 1 found in newborn screening, J. Chromatogr. B 823 (2005) 7–12.
[22] Z. Fu, M. Wang, R. Paschke, K.S. Rao, F.E. Frerman, J.J. Kim, Crystal structures of human glutaryl-CoA dehydrogenase with and without an alternate substrate: structural bases of dehydrogenation and decarboxylation reactions, Biochemistry (Mosc) 43 (2004) 9674–9684.
[23] C.T. Hsieh, W.L. Hwu, Y.T. Huang, A.C. Huang, S.F. Wang, M.H. Hu, Y.H. Chien, Early detection of glutaric aciduria type I by newborn screening in Taiwan, J. Formos. Med. Assoc. 107 (2008) 139–144.
[24] S. Kolker, S.F. Garbade, C.R. Greenberg, J.V. Leonard, J.M. Saudubray, A. Ribes, H.S. Kalkanoglu, A.M. Lund, B. Merinero, M. Wajner, M. Troncoso, M. Williams, J.H. Walter, J. Campistol, M. Marti-Herrero, M. Caswill, A.B. Burlina, F. Lagler, E.M. Maier, B. Schwahn, A. Tokatli, A. Dursun, T. Coskun, R.A. Chalmers, D.M. Koeller, J. Zschocke, E. Christensen, P. Burgard, G.F. Hoffmann, Natural history, outcome, and treatment efficacy in children and adults with glutaryl-CoA dehydrogenase deficiency, Pediatr. Res. 59 (2006) 840–847.
[25] S. Kolker, S.F. Garbade, N. Boy, E.M. Maier, T. Meissner, C. Muhlhausen, J.B. Hennermann, T. Lucke, J. Haberle, J. Baumkotter, W. Haller, E. Muller, J. Zschocke, P. Burgard, G.F. Hoffmann, Decline of acute encephalopathic crises in children with glutaryl-CoA dehydrogenase deficiency identified by newborn screening in Germany, Pediatr. Res. 62 (2007) 357–363.
[26] S. Bijarnia, V. Wiley, K. Carpenter, J. Christodoulou, C.J. Ellaway, B. Wilcken, Glutaric aciduria type I: outcome following detection by newborn screening, J. Inherit. Metab. Dis. 31 (2008) 503–507.
[27] J.D. Park, B. Lim, K.J. Kim, Y.S. Hwang, S.K. Kim, S.H. Kang, S.I. Cho, S.S. Park, J.S. Lee, J.H. Chae, Glutaric aciduria type 1 in Korea: report of two novel mutations, J. Korean Med. Sci. 25 (2010) 957–960.
[28] S. Kubo, T. Ariga, T. Okayasu, S. Arashima, K. Yuri, M. Nakayama, T. Ishii, A. Yamaguchi, Y. Kusunoki, S. Yamaguchi, Two siblings with glutaric acidemia type1, J. Jpn Pediatr. Soc. 96 (1992) 2545–2549.
[29] H. Nagasawa, S. Yamaguchi, T. Orii, M. Kobayashi, Y. Wada, K. Shikura, S. Shimao, T. Okada, Glutaric aciduria type1: four Japanese cases and their family investigation, J. Jpn Pediatr. Society. 94 (1990) 103–1808.
[30] Y. Mushimoto, Y. Hasegawa, H. Kobayashi, H. Li, J. Purevsuren, I. Nakamura, T. Taketani, S. Fukuda, S. Yamaguchi, Enzymatic evaluation of glutaric acidemia type 1 by an in vitro probe assay of acylcarnitine profiling using fibroblasts and electrospray ionization/tandem mass spectrometry (MS/MS), J. Chromatogr. B 877 (2009) 2648–2651.
[31] K.B. Bjugstad, S.I. Goodman, C.R. Freed, Age at symptom onset predicts severity of motor impairment and clinical outcome of glutaric acidemia type 1, J. Pediatr. 137 (2000) 681–686.
[32] G.F. Hoffmann, H.J. Bohles, A. Burlina, M. Duran, J. Herwig, W. Lehnert, J.V. Leonard, A. Muntau, F.K. Plecko-Starting, A. Superti-Furga, Early signs and course of disease of glutaryl-CoA dehydrogenase deficiency, J. Inherit. Metab. Dis. 18 (1995) 173–176.
[33] K.A. Strauss, E.G. Puffenberger, D.L. Robinson, D.H. Morton, Type I glutaric aciduria, part 1: natural history of 77 patients, Am. J. Med. Genet. C Semin. Med. Genet. 121 (2003) 38–52.

Molecular Genetics and Metabolism 102 (2011) 399–406

Contents lists available at ScienceDirect

Molecular Genetics and Metabolism

journal homepage: www.elsevier.com/locate/ymgme

Retrospective review of Japanese sudden unexpected death in infancy: The importance of metabolic autopsy and expanded newborn screening

Takuma Yamamoto [a], Hidekazu Tanaka [b,*], Hironori Kobayashi [c], Ko Okamura [a], Tatsuya Tanaka [d], Yuko Emoto [a], Kana Sugimoto [a,1], Masato Nakatome [a,2], Norio Sakai [e], Hisanaga Kuroki [a,3], Seiji Yamaguchi [c], Ryoji Matoba [a]

[a] Department of Legal Medicine, Osaka University Graduate School of Medicine, 2-2 Yamada-Oka, Suita, Osaka 565-0871, Japan
[b] Department of Pharmacology, Osaka University Graduate School of Medicine, 2-2 Yamada-Oka, Suita, Osaka 565-0871, Japan
[c] Department of Pediatrics, Shimane University Faculty of Medicine, 89-1 En-ya, Izumo, Shimane 693-8501, Japan
[d] Center for Medical Research and Education, Osaka University Graduate School of Medicine, 2-2 Yamada-Oka, Suita, Osaka 565-0871, Japan
[e] Department of Pediatrics, Osaka University Graduate School of Medicine, 2-2 Yamada-Oka, Suita, Osaka 565-0871, Japan

ARTICLE INFO

Article history:
Received 7 December 2010
Accepted 7 December 2010
Available online 14 December 2010

Keywords:
Sudden unexpected death in infancy
Metabolic autopsy
Expanded newborn screening
Carnitine palmitoyltransferase II deficiency

ABSTRACT

Sudden unexpected death in infancy is defined as sudden unexpected death occurring before 12 months of age. The common causes of sudden unexpected death in infancy are infection, cardiovascular anomaly, child abuse, and metabolic disorders. However, the many potential inherited metabolic disorders are difficult to diagnose at autopsy and may therefore be underdiagnosed as a cause of sudden unexpected death in infancy. In the present study we retrospectively reviewed 30 Japanese sudden unexpected death in infancy cases encountered between 2006 and 2009 at our institute. With postmortem blood acylcarnitine analysis and histological examination of the liver, we found two cases of long-chain fatty acid oxidation defects. Molecular analysis revealed that the one patient had a compound heterozygote for a novel mutation (p.L644S) and a disease-causing mutation (p.F383Y) in the *carnitine palmitoyltransferase 2* gene. Furthermore, retrospective acylcarnitine analysis of the newborn screening card of this patient was consistent with carnitine palmitoyltransferase II deficiency. Metabolic autopsy and expanded newborn screening would be helpful for forensic scientists and pediatricians to diagnose fatty acid oxidation disorders and prevent sudden unexpected death in infancy.

1. Introduction

Sudden unexpected death in infancy (SUDI) is defined as sudden unexpected death occurring before 12 months of age. If SUDI remains unexplained after thorough investigations, it is labeled sudden infant death syndrome (SIDS). The common causes of SUDI are infection, cardiovascular anomaly, child abuse, and metabolic disorders. However, the many potential inherited metabolic disorders are more difficult to diagnose at autopsy than cardiovascular defects and serious infection. They may, therefore, be underdiagnosed as a cause of SUDI or misdiagnosed as SIDS [1,2]. Fatty acid oxidation disorders (FAODs) are one type of the inherited metabolic disorders and may cause as much as 5% of SUDI cases after thorough investigations including metabolic autopsy [3–7]. In Japan, however, not all SUDI cases have been subjected to metabolic autopsy and postmortem diagnosis of FAODs is infrequent. Therefore, the proportion of FAODs to SUDI is currently unknown.

Many FAODs are inherited in an autosomal recessive manner and are thus associated with a high risk of recurrence in siblings. Undiagnosed siblings are also therefore at risk of sudden death. Moreover, some FAODs can be treated if diagnosed accurately, so early diagnosis may prevent sudden death. Accurate diagnosis of FAODs is consequently important for genetic counseling as well as for the treatment of the infants.

One of the most common causes of FAODs is deficiency of the carnitine palmitoyltransferase (CPT) enzyme system, which transfers long-chain fatty acids, containing 16 carbons or more (C16, C18:1, C18:2, and C18), from the cytosolic compartment to the mitochondrial matrix, where β-oxidation takes place. The CPT enzyme system consists of several mitochondrial membrane-bound enzymes: CPT I, CPT II (EC2.3.1.21) and carnitine-acylcarnitine translocase (CACT). Among them, CPT II deficiency is the most common. CPT II is situated on the inner aspect of the inner mitochondrial membrane and converts long-chain acylcarnitines to long-

Abbreviations: CACT, carnitine-acylcarnitine translocase; CPT II, carnitine palmitoyltransferase II; FAOD, fatty acid oxidation disorder; LCHAD, long-chain hydroxyacyl-CoA dehydrogenase; MTP, mitochondrial trifunctional protein; SIDS, sudden infant death syndrome; SUDI, sudden unexpected death in infancy; VLCAD, very-long-chain acyl-CoA dehydrogenase.

* Corresponding author. Fax: +81 6 6879 3529.
E-mail address: htanaka@pharma1.med.osaka-u.ac.jp (H. Tanaka).
[1] Present address: Department of Molecular and Cellular Physiology, Graduate School of Medicine, Ehime University, Toon, Ehime 791-0295, Japan.
[2] Present address: Department of Legal Medicine, Fujita Health University School of Medicine, 1-98 Dengakugakubo, Kutsukake, Toyoake, Aichi 470-1192, Japan.
[3] Present address: Graduate School of Risk & Crisis Management Study, Chiba Institute of Science, 15-8 Shiomi-cho, Choshi, Chiba 288-0025, Japan.

1096-7192/$ – see front matter © 2010 Elsevier Inc. All rights reserved.
doi:10.1016/j.ymgme.2010.12.004

chain acyl-CoAs. CPT II deficiency induces the accumulation of long-chain fatty acids, which causes fatty degeneration in liver and vacuolization in hepatocytes. Hepatic steatosis is therefore a constant feature [8–10].

CPT II deficiency is categorized into three forms: neonatal (OMIM 608836) [11–13], infantile (OMIM 600649) [14], and adult (OMIM 255110) [15]. The infantile form usually manifests between 6 and 24 months of age. It shows recurrent attacks of hypoketotic hypoglycemia resulting in coma and seizures, liver failure, and transient hepatomegaly. About half of the cases have heart involvement with cardiomyopathy and arrhythmia, and some cases result in SUDI [8–10,16,17].

In the present study we retrospectively reviewed 30 Japanese SUDI cases encountered between 2006 and 2009 at our institute. With postmortem blood acylcarnitine analysis and histological examination of the liver, we found two cases of long-chain fatty acid oxidation defects. Molecular analysis revealed that the one patient had a compound heterozygote for a novel mutation (p.L644S) and a disease-causing mutation (p.F383Y) in the *CPT 2* gene. Furthermore, retrospective acylcarnitine analysis of the newborn screening card of this patient was consistent with CPT II deficiency.

2. Materials and methods

2.1. Subjects

Between 2006 and 2009, forensic autopsy was performed on 923 cases at our institute, 50 of whom were under 12 months of age. Following macroscopic examination, 20 cases could be diagnosed but 30 cases (Table 1) did not have any characteristic appearance and remained undiagnosed. For this study we retrospectively reviewed these 30 undiagnosed cases with age ranging from 1 day to 10 months (males: 17, females: 13).

2.2. Sudan III staining

Liver samples preserved in 4% phosphate-buffered formaldehyde solution were frozen, cut into 10-μm sections, and stained by the Sudan III method for fat staining.

2.3. Postmortem blood acylcarnitine analysis by tandem mass spectrometry

Frozen whole blood samples which had been obtained at autopsy were thawed and blotted onto one spot on Guthrie cards and then subjected to acylcarnitine analyses by tandem mass spectrometry.

2.4. Extraction of genomic DNA and mutational analysis

Genomic DNA was purified from frozen blood samples with the PureLink™ Genomic DNA kit (Invitrogen, Grand Island, NY) according to the manufacturer's instructions. Each of the exons with their respective flanking intronic regions was then amplified, followed by polymerase chain reaction (PCR) performed in a 25-μL volume containing 12.5 μL of PrimeSTAR Max Premix (2×) (Takara, Otsu, Japan), 0.4 μM each of the primers (*CPT 2*: Table 2, *SLC25A20* (hereafter called *CACT*), *ACADVL*, *HADHA*, and *HADHB*: not shown) and 200 ng of template DNA under the following conditions: 98.0 °C for 1 min, (98.0 °C for 10 s, 54.0 °C for 5 s, 72.0 °C for 30 s) for 30 cycles, and 72.0 °C for 5 min. PCR products were sequenced with the BigDye® Terminator v3.1 Cycle Sequencing Kit (Applied Biosystems, Foster City, CA) on the Applied Biosystems 3730 DNA Analyzer (Applied Biosystems) according to the manufacturer's instructions. Sequences from the 5′ ends were confirmed by comparison with those from the 3′ ends at least twice independently, and each sequence was compared with the standard sequence (GenBank accession number:

Table 1
SUDI cases.

Case no.	Age/sex	Height/weight (cm/kg)	Circumstances	Fever	Steatosis	Acylcarnitine profiles	Remarks
1	6 months/M	70/9.4	Awake	+	Distinctive	CPT II deficiency CACT deficiency	
2	5 d/F	54/3.7	Sleeping	−	Moderate	LCFAO defects	
3	1 months/M	59/5.7	Awake	−	Moderate	No specific change	
4	1 d/M	45/2.6	Sleeping	−	Normal	No specific change	Cesarean section
5	10 d/F	51/3.1	Unknown	−	Normal	No specific change	
6	22 d/M	61/4.8	Sleeping	−	Normal	No specific change	Cesarean section, transient tachypnea of the newborn
7	25 d/M	NR/NR	Unknown	−	Normal	No specific change	
8	25 d/F	48/3.6	Sleeping	−	Normal	No specific change	Induction
9	25 d/M	57/3.6	Sleeping	+	Normal	No specific change	
10	1 months/F	53/4.0	Sleeping	−	Normal	No specific change	Sister: SUDI
11	1 months/F	55/3.5	Sleeping	−	Normal	No specific change	Cesarean section, transient tachypnea of the newborn
12	2 months/M	58/5.7	Sleeping	−	Normal	No specific change	
13	2 months/M	59/6.2	Sleeping	+	Normal	No specific change	Cesarean section
14	2 months/F	57/5.0	Sleeping	−	Normal	No specific change	
15	3 months/M	61/5.0	Sleeping	−	Normal	No specific change	
16	4 months/M	73/7.9	Sleeping	−	Normal	No specific change	
17	4 months/M	63/7.4	Sleeping	+	Normal	No specific change	
18	4 months/M	59/5.1	Sleeping	−	Normal	No specific change	
19	4 months/F	61/6.1	Sleeping	−	Normal	No specific change	
20	4 months/M	66/7.2	Sleeping	−	Normal	No specific change	
21	5 months/F	66/6.3	Sleeping	+	Normal	No specific change	Cesarean section
22	6 months/F	62/7.6	Sleeping	+	Normal	No specific change	Rotavirus
23	6 months/M	64/8.6	Sleeping	−	Normal	No specific change	Cesarean section
24	7 months/F	62/7.0	Sleeping	+	Normal	No specific change	
25	7 months/M	70/8.5	Awake	+	Normal	No specific change	
26	7 months/F	67/6.7	Sleeping	−	Normal	No specific change	Cesarean section
27	7 months/F	64/6.7	Sleeping	−	Normal	No specific change	
28	8 months/F	70/9.7	Sleeping	−	Normal	No specific change	
29	9 months/M	74/NR	Sleeping	−	Normal	No specific change	
30	10 months/M	74/8.0	Sleeping	−	Normal	No specific change	Ventricular septal defect

Abbreviations: d, days; F, female; LCFAO defects: Long-chain fatty acid oxidation defects; M, male; NR, not recorded.

Table 2
Nucleotide sequences of PCR primers used for the *CPT 2* gene sequencing.

Primer name	Primer sequence
CPT2-F1	5′-CTTGTGTTTAGACTCCAGAACTCCC-3′
CPT2-R1	5′-GTCATGAGTGACTGCAGTCAGGTTG-3′
CPT2-F2	5′-GATCTAGTAATCAGTTCATT-3′
CPT2-R2	5′-AGGTTCTGGGTTCCTGGAGA-3′
CPT2-F3	5′-TTCCAGGTTTTAGGGCTATG-3′
CPT2-R3	5′-GGAGGATGAGACGTTACTTC-3′
CPT2-F4a	5′-TAGGGACAGCATTAACATTT-3′
CPT2-R4a	5′-TGGCCTTGTCAGTGAAG-3′
CPT2-F4b	5′-GTCCCAGTATTTTCGGCTTT-3′
CPT2-R4b	5′-TGTGGGACAAGTGGACAAGG-3′
CPT2-F4c	5′-CAGTGTTCTGTCTCTGCCTA-3′
CPT2-R4c	5′-GCCTCCTCTCTGAAACTGGA-3′
CPT2-F4d	5′-ACAGCTGCTAAGGAAAAGTT-3′
CPT2-R4d	5′-CAAGACCCAAGGGCATGCTC-3′
CPT2-F5	5′-CTGAGACTCTGGTTTTCCAT-3′
CPT2-R5	5′-GGTAGCTTTTCATCTGCCCA-3′

Abbreviations: F, forward; R, reverse.

CPT 2: NM_000098.2, *CACT*: NM_000387.4, *ACADVL*: NM_000018.2, *HADHA*: NM_000182.4 and *HADHB*:NM_000183.2).

2.5. Haplotype analysis of the CPT 2 gene

The 3304-bp PCR products were amplified with a pair of primers (CPT2-F4b and CPT2-R5; Table 2), which include a pair of heterozygous mutations (c.1148T>A on exon 4 and c.1931T>C on exon 5). PCR was performed under the following conditions: 98.0 °C for 1 min, (98.0 °C for 10 s, 54.0 °C for 5 s, 72.0 °C for 3 min) for 30 cycles, and 72.0 °C for 5 min. Next, we performed reconditioning PCR [18] in order to avoid heteroduplexes from mixed-template PCR products. After the PCR products were obtained, they were diluted 10-fold into a fresh reaction mixture of the same composition and cycled three times [18]. The 3304-bp PCR products were purified from agarose gel and cloned into the pCR®-Blunt II-TOPO® vector (Invitrogen, Grand Island, NY), and the resulting constructs were transformed into the Competent high DH5α (Toyobo, Osaka, Japan). Colonies were selected and analyzed on kanamycin agar and the plasmid inserts were sequenced by using the M13 Forward primer and the M13 Reverse primer (Invitrogen).

2.6. Genotyping of healthy individuals

One hundred chromosomes from healthy Japanese volunteers were subjected to genotyping by direct sequencing in the same manner as described above.

2.7. Acylcarnitine analysis of newborn screening card by tandem mass spectrometry

The newborn screening card of case 1 was obtained. It was subjected to acylcarnitine analysis by tandem mass spectrometry.

2.8. Ethics

This study was approved by the Ethics Committee of the Osaka University Graduate School of Medicine.

3. Case histories

3.1. Case 1

The patient was the full-term male product of a normal pregnancy. His Apgar score was 9, birth weight was 3148 g, length was 51 cm, and head circumference was 33.5 cm. Family history was negative for seizures, arrhythmias, and sudden death, and he had a healthy 2-year-old brother. His parents were not consanguineous.

At 6 months of age, he was taken to a doctor's office because of a fever that had continued for a few days and acetaminophen was prescribed. However, in the evening of the same day he suddenly lost consciousness and an ambulance was called soon afterwards. However, when the emergency service personnel arrived, he had suffered cardiopulmonary arrest. Although cardiopulmonary resuscitation was initiated immediately and continued after he reached the hospital, he was pronounced dead.

3.2. Case 2

The patient was the full-term female product of a normal pregnancy. Her birth weight was 3884 g. Family history was negative for seizures, arrhythmias, and sudden death, and she had a healthy 5-year-old brother and 4-year-old sister. Her parents were not consanguineous.

At 5 days of age, in the morning, she was found to have undergone cardiopulmonary arrest during sleep at home. Although cardiopulmonary resuscitation was initiated immediately and she was delivered to a hospital, she was pronounced dead.

3.3. Case 3

The patient was born at term weighing 2664 g as the first child to no consanguineous parents. His birth length was 48.7 cm and head circumference was 33.0 cm. His father was 29-year-old and had arrhythmia.

At 53 days of age, after he drank milk, he suddenly lost consciousness and respiration was arrested. An ambulance was called soon afterwards but when the emergency service personnel arrived, he had suffered cardiopulmonary arrest. He was delivered to a hospital and intensive critical care was performed, only to be pronounced dead at the emergency room.

4. Results

4.1. Histological examination

One of the important features in diagnosing FAODs is hepatic steatosis, which represents the accumulation of fatty acids. We therefore performed Sudan III staining to examine whether vacuoles caused by fatty degeneration were presented in hepatocytes. Diffuse and distinctive Sudan III-positive vacuoles were detected in case 1 (Fig. 1A) and moderate Sudan III-positive vacuoles were detected in cases 2 and 3 (Fig. 1B and C). No Sudan III-positive vacuoles were detected in the other cases, for example case 11 (Fig. 1D).

4.2. Postmortem blood acylcarnitine analysis

We performed acylcarnitine analyses by tandem mass spectrometry using whole blood samples. In most of the postmortem samples, free carnitine and short-chain acylcarnitines were increased (Supplementary data). In almost all cases the data were within the third quartile + 1.5 of the interquartile range (IQR), whereas the long-chain acylcarnitines in cases 1 and 2 were distinctly increased (Fig. 2). These data suggested that cases 1 and 2 were affected by long-chain fatty acid oxidation defects.

In case 1, long-chain acylcarnitines such as C16, C18:1, C18:2, and C18 were increased, but C14:1 and C14:2 were not increased. The ratio of C16 to C14:1 was as high as 49.4. This suggests that case 1 had CPT II deficiency or CACT deficiency.

In case 2, not only C16, C18:1, C18:2, and C18 but also C14:1 and C14:2 were increased. The ratio of C16 to C14:1 was 16.25. Long-chain hydroxyacylcarnitines such as C16:OH, C18:1OH, and C18:OH were also increased. These data suggest that case 2 had long-chain fatty acid oxidation defects such as long-chain hydroxyacyl-CoA dehydrogenase (LCHAD) deficiency or mitochondrial trifunctional protein (MTP) deficiency.